Synthesis of *β*-myrcene-based polymers and styrene block and statistical copolymers by SG1 nitroxide-mediated controlled radical polymerization

Adrien Métafiot,[†,φ,‡] Yara Kanawati,[†] Jean-François Gérard,[φ] Brigitte Defoort,[‡] and Milan Marić*,[†]

[†]Department of Chemical Engineering, McGill University, 3610 University St., Montreal, H3A 2B2 Quebec, Canada

[φ]Ingénierie des Matériaux Polymères (IMP), CNRS UMR5223, INSA – Lyon, 17 Jean Capelle Avenue, 69621 Villeurbanne, France

[‡]Airbus Safran Launchers (ASL), 78130 Les Mureaux, France

Keywords: *β*-myrcene; styrene; nitroxide-mediated polymerization; copolymerization

ABSTRACT. Nitroxide-mediated polymerization (NMP) of *β*-myrcene (*My*) at 120 ºC in bulk using unimolecular SG1-based succinimidyl ester-functionalized BlocBuilder[TM] alkoxyamine resulted in low dispersity (Đ = 1.1-1.4) poly(myrcene)s P(*My*)s with high SG1 chain end fidelity.

The polymerizations also showed the number-average molecular weights (M_n) increased almost linearly with conversion. SG1-terminated P(My) macroinitiators were cleanly chain-extended with styrene (S) and the S-rich P(My-b-S) diblock copolymers exhibited two distinct glass transition temperatures (T_gs), indicative of micro-phase separation. P(My-b-S) diblocks showed brittle stress-strain behavior, plausibly due to relatively low M_n. My/S mixtures, with initial S molar feed compositions $f_{S,0}$ = 0.10-0.94 were also statistically copolymerized (M_n = 8.2-19.8 kg.mol^{-1}, Đ ≤ 1.37 and monomodal distributions). Copolymer reactivity ratios were r_S = 0.25 ± 0.04 / 0.34 ± 0.19 and r_{My} = 1.88 ± 0.12 / 2.19 ± 0.07 using Fineman-Ross and Kelen-Tüdös methods. The statistical P(My-$stat$-S) copolymers displayed a range of T_gs (− 77 to + 30 ℃) depending on My molar fraction. My-rich and S-rich P(My-$stat$-S)s were then successfully chain-extended with both S and My.

INTRODUCTION. Terpenes are hydrocarbons that contain one or more carbon–carbon double bonds and share the same elementary unit as isoprene. They are a class of important bio-derived compounds[1,2] and have been known for hundreds of years as components of essential oils obtained from leaves, flowers, and fruits of many plants[3]. Among the vast members of the terpene family, $β$-myrcene (7-methyl-3-methylene-octa-1,6-diene, abbreviated My) particularly is an interesting "renewable" monomer, as it is a component of the bay, ylang–ylang, wild thyme, lemon grass, and juniper berry essential oils[3]. It is an acyclic monoterpene with a highly active conjugated diene structure that can be polymerized by classical polymerization methods. Based upon its relatively low cost[3] and ease of isolation[4-8], My has been studied quite extensively as a starting material for polymers. Similar to other 1,3-dienes, such as butadiene and isoprene, My

also forms rubbery polymers when polymerized. It is either used in small amounts as an additive to adjust elastomeric properties, or as a main component in poly(myrcene)s P(*My*)s[3]. For instance, the syntheses of styrene/*β*-myrcene (S/*My*) copolymers and *My*-based composites showed that the use of *My* improved the mechanical properties of poly(styrene)-based plastics[9]. Likewise, Cawse and coworkers incorporated hydroxyl-functionalized P(*My*) into a poly(urethane) leading to improved stress-strain behavior and impact properties[10]. Hence, *My*, either as a homopolymer or when copolymerized with another monomer, can provide a wide latitude of polymer properties. *My*'s polymerization was comprehensively studied by conventional free radical polymerization[11-16]. Coordination polymerization was also applied to this acyclic conjugated diene. For example, Loughmari and Georges et al. reported stereoselective polymerization of *My* utilizing a lanthanide-based catalyst[17]. Living or quasi-living ionic polymerizations of *My* have been explored as well. For instance, Sivola et al reported the synthesis of living P(*My*)s via anionic polymerization initiated by *n*-butyllithium (*n*-BuLi)[18]. This approach allows manufacturing tailor-made macromolecules with precise and pre-determined molar masses, compositions, topologies and functionalities. P(*My-b*-S) triblock copolymer, which could be used as a thermoplastic elastomer, was made in this way by Quirk et al[19,20]. Hoye and Hillmyer reported a similar polymer combined with bio-based *α*-methyl-*p*-methylstyrene prepared by the dehydrogenation of limonene[21]. In spite of these successful outcomes by living anionic polymerization, this technique exhibits one main disadvantage which is the requirement of stringent reaction conditions, especially the use of chemically ultrapure reagents as well as the absolute removal of air and of traces of water[22]. Polymer chemists have long desired to develop polymerization processes that combine the control of microstructure

typified by ionic polymerization but with the ease of industrial implementation typified by other types of polymerization such as free radical or addition polymerization.

The advances in macromolecular synthesis in the last two decades provided a game-changing synthetic tool to easily achieve complex macromolecular architectures: reversible-deactivation radical polymerization (RDRP)[23-27]. In comparison to living anionic and cationic polymerizations, RDRP differs by its relative ease-of-use since only dissolved oxygen has to be eliminated, it can polymerize a wide variety of vinylic monomers by a radical mechanism that are not possible ionically, and the latitude in process conditions possible (bulk, solution, emulsion, dispersion, etc.)[28]. The three major families of RDRP are nitroxide-mediated polymerization (NMP)[25,26,29], atom transfer radical polymerization (ATRP)[24,30-32] and reversible addition fragmentation transfer polymerization (RAFT)[23,33-35].

RDRP applied to My is a great opportunity to produce high value-added polymers with a segment based on renewable monomers. Surprisingly enough, RDRP-based P(My) has not been synthesized and characterized prior to 2015. Very recently, the first RDRP of My was successfully performed by RAFT[36]. However, NMP has so far never been applied for My polymerization, whereas this process exhibits some advantages: NMP does not rely on sulfur-based chain transfer agents like RAFT does or metallic ligands that ATRP required, which may contaminate polymers for some applications[37,38]. NMP is historically the first and represents perhaps the easiest RDRP technology to apply as the initiators and mediators are directly available from commercial sources. Although the synthesis of this poly(terpene) by NMP has not been studied yet, other 1,3-diene monomers were polymerized in a controlled manner. Indeed, isoprene and butadiene were successfully polymerized by NMP. The achievement of relatively broad molecular weight distribution NMP-based polyisoprenes (Đ = M_w/M_n, dispersity of 1.36-

1.53) with the use of TEMPO, the first-generation stable nitroxide, was reported in the late 1990s[39,40]. Hawker and co-workers used then a TIPNO-based initiator, 2,2,5-trimethyl-3-(1-phenylethoxy)-4-phenyl-3-azahexane to produce polyisoprenes and polybutadienes with relatively high number-average molar masses (M_n > 80 000 g.mol^{-1}) and narrow molecular weight distributions (Đ < 1.3)[41]. Grubbs et al synthesized a well-defined poly(isoprene) sample (Đ = 1.28) using 2,2-dimethyl-3-(1-phenylethoxy)-4-phenyl-3-azapentane alkoxyamine produced by the addition of two equivalents of 1-phenylethyl radical to 2-methyl-2-nitrosopropane[42]. They also reported the NMP of isoprene using a poly(ethylene oxide)-alkoxyamine macroinitiator, resulting in diblock copolymers with narrow molecular weight distributions (Đ < 1.20) characteristic of living chain growth processes[43]. The discovery of more labile second-generation initiators exhibiting a lower energy C-ON bond homolysis[44,45] such as 2,2,5-trimethyl-4-phenyl-3-azahexane-N-oxyl (TIPNO)[46] and [*tert*-butyl[1-(diethoxyphosphoryl)-2,2-dimethylpropyl]amino] nitroxide, termed DEPN or SG1[47] (Figure 1,1) allowed controlled polymerizations at lower temperatures. One of the most predominant alkoxyamine unimolecular initiators based on SG1 is 2-([*tert*-butyl[1-(diethoxyphosphoryl)-2,2-dimethylpropyl]amino]oxy)-2-methylpropionic acid termed BlocBuilder^{TM} (Figure 1,2). Initiators containing the SG1 moiety have high dissociation rate constants[45] giving excellent control over the homopolymerizations of 1,3-dienes[48] and many other monomers such as acrylates[49-52]. Harrisson and coworkers reported for the first time the NMP of isoprene from a range of SG1-based initiators[53]. Well-controlled poly(isoprene)s were obtained without addition of extra SG1. At higher conversions, the dispersity of all synthesized poly(isoprene)s approached 1.1.

Given the positive results achieved previously with isoprene and butadiene using BlocBuilder[TM] type initiators, the NMP-based *My* chemistry appears very promising. Furthermore, *My* exhibits two valuable features in comparison to isoprene and butadiene: It is a natural renewable compound with low volatility (boiling point T_b = 167 °C)[3], meaning that pressurized equipment is not needed to handle it.

In the present study, we report first the effects of target number-average molecular weight ($M_{n,theo}$), reaction medium, temperature and additional SG1 free nitroxide on the control of NMP of *My*. A BlocBuilder[TM]-modified initiator, the succinimidyl ester terminated NHS-BlocBuilder (NHS-BB, Figure 1,3)[54-57] was used during this study and the relevance of this choice is explained below in the discussion. The optimized reaction conditions were used to chain-extend cleanly P(*My*)-SG1 macroinitiator with a fresh batch of S. Thermal and stress-strain properties of the resulting P(*My-b-*S) diblock copolymer were also investigated. Further, NHS-BB initiated the copolymerization of *My* and S via NMP was studied in terms of reactivity ratios and the resulting glass transition temperatures of the copolymers. To the best of our knowledge, this paper is the first comprehensive kinetic investigation of the nitroxide-mediated (co-)polymerization of *My* leading to well-defined P(*My*) homopolymers, P(*My-b-*S) diblock copolymers and P(*My-stat-*S) statistical copolymers.

1   2   3
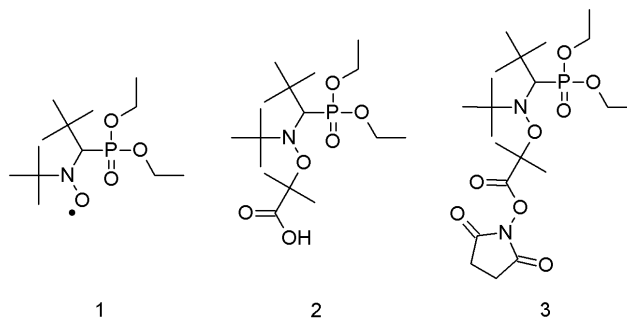
Figure 1. Structure of the *N-tert*-butyl-*N*-[1-diethylphosphono-(2,2-dimethylpropyl)] nitroxide (SG1, **1**), of the 2-([*tert*-butyl[1-(diethoxyphosphoryl)-2,2-dimethylpropyl]amino]oxy)-2-methylpropionic acid alkoxyamine (BlocBuilder™, **2**) and of the succinimidyl ester terminated NHS-BlocBuilder

EXPERIMENTAL SECTION.

◘ Materials.

β-Myrcene (*My*, ≥ 90 %), basic alumina (Al$_2$O$_3$, Brockmann, Type I, 150 mesh), calcium hydride (CaH$_2$, 90-95 % reagent grade) and 1,4-dioxane (≥ 99 %) were purchased from Sigma-Aldrich and used as received. Toluene (≥ 99 %), methanol (MeOH, ≥ 99 %) and tetrahydrofuran (THF, 99.9 % HPLC grade) were obtained from Fisher Scientific and used as received. 2-Methyl-2-[*N-tert*-butyl-*N*-(1-diethoxyphosphoryl-2,2-dimethylpropyl)-aminoxy]–*N*-propionyloxy-succinimide, also known as NHS-BlocBuilder (NHS-BB), was prepared according to a published method[53] from 2-(*tert*-butyl[1-(diethoxyphosphoryl)-2,2-dimethylpropyl]aminooxy)-2-methylpropionic acid, also known as MAMA-SG1 (BlocBuilder™, 99 %, purchased from Arkema and used without further purification), *N*-hydroxy-succinimide

(NHS, 98 %, purchased from Aldrich and used as received) and *N,N'*-dicyclohexylcarbodiimide (DCC, 99 %, purchased from Aldrich and used as received). *N-tert*-Butyl-*N*-[1-diethylphosphono-(2,2-dimethylpropyl)] nitroxide (SG1, > 85 %) was kindly donated by Noah Macy of Arkema and used as received. Styrene (S, 99 %) was obtained from Fisher Scientific and was purified to remove the inhibitor (*p-tert*-butylcatechol) by passing through a column of basic alumina mixed with 5 weight % calcium hydride and then stored in a sealed flask under a head of nitrogen in a refrigerator until needed. The deuterated chloroform (CDCl$_3$, 99.8 %) used as a solvent for proton and carbon nuclear magnetic resonance (^{1}H and ^{13}C NMR) was obtained from Cambridge Isotopes Laboratory.

◘ **(Co-)Polymerization of *β*-myrcene (with styrene) by NMP.**

The (co-)polymerizations were performed in a 25-mL three-necked round-bottom glass flask equipped with a reflux condenser, a thermal well and a magnetic stir bar. The flask was placed inside a heating mantle and the whole set-up mounted on top of a magnetic stirrer. Table 1 and Table 5 list the formulations studied for the various *My*(/S) (co-)polymerizations. For example, for the experiment *My*/S-20 (molar fraction of S in the initial feed $f_{S,0} = 0.20$), the reactor was sealed with the rubber septa after the addition of NHS-BB (0.204 g, 0.427 mmol) and the stir bar. *My* (10.514 g, 77.178 mmol) and previously purified S (2.043 g, 19.616 mmol) were then injected with a disposable needle into the reactor. For this experiment, the initial molar ratio of monomers and NHS-BB was calculated to give theoretically a *My*/S copolymer sample with target number-average molecular weight $M_{n,theo} = (M_{My}f_{My,0} + M_S f_{S,0})$ DP = 30 kg.mol^{-1} at

complete overall conversion with DP = $([My]_0 + [S]_0) / [NHS\text{-}BB]_0 = 231$, the average degree of polymerization.

A thermocouple connected to the temperature controller was placed inside the thermal well and connected through one of the necks. A mixture of ethylene glycol/distilled water (20/80 vol%) at a temperature of 5 °C was circulated (Fisher Scientific Isotemp 3016D Digital Refrigerated Bath) through the condenser connected to one of the necks of the reactor to prevent any evaporation loss of the monomers. A purge of ultra-pure nitrogen was then introduced to the reactor for 30 min to deoxygenate at room temperature the reactants prior to polymerization. The purge was vented through the reflux condenser. After purging, the reactor was heated at a rate of about 10 °C.min^{-1} to the desired polymerization temperature (T = 120 °C for My/S-20) with continuous nitrogen purge. The time at which the reactor temperature reached 100 °C was taken arbitrarily as the commencement of the reaction ($t = 0$ min). Samples were then taken from the reactor periodically by a syringe until the end of the experiments or until the samples became too viscous to withdraw. Reactions were then stopped by removing the reactor from the heating mantle and letting the contents cool down to room temperature, while under continuous nitrogen purge. For each sample withdrawn during the polymerization, the crude polymer was precipitated with excess methanol. After filtration and recovery, the precipitated polymer was dried at 40 °C under vacuum in the oven overnight to remove unreacted monomers. Samples were analyzed by nuclear magnetic resonance (NMR) and gel permeation chromatography (GPC). Specifications of the GPC and the NMR are fully described in the Characterization section. At the end of the experiment, the overall NMR conversion for My/S-20 was 37.1 % (individual conversions: $X_{My} = 40.5$ % and $X_S = 28.9$ %) with $M_n = 9.9$ kg.mol^{-1}, molecular weight distribution Đ = 1.26 and the molar composition of S in the final copolymer was $F_S =$

0.15 according to NMR spectroscopy. The exact same procedure was followed for all My/S copolymerizations and My homopolymerizations.

�‌ **Chain-extension of poly(myrcene) P(My) homopolymer macroinitiator and poly(myrcene-*stat*-styrene) P(My-*stat*-S) statistical copolymer macroinitiator with styrene and/or *β*-myrcene.**

P(My) homopolymers and P(My-*stat*-S) statistical copolymers were chain-extended with purified S and/or My at 110 °C or 120 °C in 50 wt% toluene solution or in bulk. The experimental setup and procedures were the same as the syntheses for the P(My) and P(My-*stat*-S) polymers described earlier. The entire set of formulations for the chain-extension experiments is shown in Table 3, from P(My) macroinitiators, and Table 7.B, from P(My-*stat*-S) macroinitiators. An example is given to illustrate the chain-extension of My/S statistical copolymer macroinitiator with purified S. To the reactor was added My/S-20 macroinitiator (1.00 g, M_n = 9.9 kg.mol^{-1}, Đ = 1.26) and toluene (7.51 g, 81.51 mmol) solvent with magnetic stirring. After sealing the reactor, previously purified S (6.49 g, 62.31 mmol) was added via syringe and a purge of nitrogen was applied for 30 minutes. The reactor was then heated to 110 °C to commence polymerization while continuing the nitrogen purge. Samples were periodically removed by syringe and polymers were precipitated using excess methanol. After removal of the supernatant, the wet cake was dried under vacuum at 50 °C to obtain the My/S-20-S block copolymer. The chain-extended products were characterized by GPC, calibrated with poly(styrene) PS standards, at 40°C in THF eluent. For the specific example cited, the final S

conversion was 53 % according to ^{1}H NMR spectroscopy with M_n = 25.3 kg.mol^{-1} and dispersity Đ = 1.46 determined by GPC.

◻ **Characterization.**

The overall monomer conversion X was determined by gravimetry X_{grav} and ^{1}H nuclear magnetic resonance (NMR) X_{NMR} (average deviation = 3.12 %, standard deviation = 2.48 %, see Supporting Information for Xgrav and X_{NMR} values in the course of experiment *My*-6, Figure S1) and calculated from formula 1:

$$X = (X_{grav} + X_{NMR}) / 2 \quad (1)$$

X_{grav} was calculated from the following formula:

$$X_{grav} = (m_{v+p} - m_v) / [(m_{v+p+s} - m_v) \times (100 - w_S)] \quad (2)$$

in which m_v is the mass of the empty vial, m_{v+p+s} is the mass of the vial containing the reaction solution just after the sample withdrawal (polymer, unreacted monomer(s) and solvent if used), m_{v+p} is the mass of the vial containing the polymer after drying and w_S is the mass percentage of solvent relative to the initial masses of initiator and monomer(s). In order to prevent any overestimated X_{grav}, drying of the samples was performed first under intense air flow for 24 h and then under vacuum at 50 °C for 24 h to maximize the removal of non-polymer components.

Average conversion X_{NMR} was then calculated from formula 3:

$$X_{NMR} = X_{My} f_{My,0} + X_S f_{S,0} \quad (3)$$

where $f_{My,0}$ and $f_{S,0}$ are the initial molar fractions of *My* and S respectively and X_{My} and X_S are the individual conversions of *My* and S respectively. X_{My} and X_S were determined with a Varian NMR Mercury spectrometer (^{1}H NMR, 300 MHz, 32 scans) using CDCl$_3$ deuterated solvent. The signal of the solvent (δ = 7.27 ppm) was used as reference for chemical shifts. *My* conversion was calculated by comparing the integrated peaks corresponding to the four aliphatic protons of the monomers (δ = 2.15-2.30 ppm), the eight aliphatic protons of the polymers (δ = 1.90-2.15 ppm) and the six protons of the two methyl groups of both monomers and polymers (δ = 1.55-1.75 ppm). S conversion was determined using the three vinyl protons (δ = 6.7-6.8, 5.7-5.8 and 5.2-5.3 ppm) of the monomers and the five aromatic protons of both monomers and polymers (δ = 6.9-7.5 ppm). Please note that X was only used for homopolymerizations. In the case of the copolymerizations, X_{NMR} was considered since *My* and S have significantly different molar masses.

The regioselectivity of the *My* repetitive units in the various *My*-based polymers was also determined by using the same spectra (^{1}H NMR, 300 MHz Varian NMR Mercury spectrometer, CDCl$_3$ eluent, 32 scans). Comparing the three integrated peaks at δ = 4.70-4.80 ppm (two vinyl protons of 3,4-addition and two vinyl protons of 1,2-addition), δ = 5.00-5.25 ppm (two olefinic protons of 1,4-addition, one olefinic proton of 1,2-addition and one olefinic proton of 3,4-addition) and δ = 5.30-5.50 ppm (one olefinic proton of 1,2-addition) allowed the three different types of configurations to be quantified[16]. The two stereoisomers of 1,4-P(*My*), *cis*-1,4-P(*My*) and *trans*-1,4-P(*My*), were quantified using ^{13}C NMR (300 MHz Varian NMR Mercury spectrometer, CDCl$_3$ eluent at δ = 77.4 ppm, 1000 scans) chemical shifts of specific nuclei: methylene carbon at δ = 37-38 ppm (*trans*-, 37,6 ppm; *cis*-, 37.1 ppm) and the quaternary carbon at δ = 131-132 ppm (*trans*-, 131.7 ppm; *cis*-, 131.3 ppm)[58]. Deconvolution (Mnova® software,

GSD options, 5 fitting cycles with high resolution, proportional line width new spectrum with factor 0.30) was applied to all ^{13}C NMR spectra in order to improve the quality of the integrations.

Two P(*My-stat*-S) copolymers were analyzed by ^{31}P NMR spectroscopy to determine the fraction of the chains terminated with SG1. The spectra were recorded in CDCl$_3$ using a 5 mm diameter Up NMR tube with 800 scans being performed in a 200 MHz Varian Gemini 2000 spectrometer operating at 81 MHz. The NMR tubes were carefully weighed and filled with polymer (mass of polymer = 0.0682 g and 0.1179 g for *My*/S-07 with M_n = 11.1 kg.mol^{-1} and *My*/S-55 with M_n = 16.6 kg.mol^{-1} respectively) and diethylphosphite as internal reference (0.0044 g and 0.0031 g respectively). In order to know if *My*-based polymers and diethylphosphite have similar relaxation times, *My*/S-55 was run under the exact same conditions with only one scan and no dummy scans (ss = 0). A negligible difference (< 1.9 %) in integral values was measured between this spectrum and the standard one with multiple scans. It was thereby assumed that diethylphosphite and *My*-based polymers with moderate M_n < 17 kg.mol^{-1} relax at the same rate.

The number-average molecular weights ($M_{n,GPC}$) and the molecular weight distributions (Đ = M_w/M_n) were measured using gel permeation chromatography (GPC, Water Breeze) with HPLC grade tetrahydrofuran (THF) as the mobile phase. A mobile phase flow rate of 0.3 mL.min^{-1} was applied and the GPC was equipped with 3 Waters Styragel® HR columns (HR1 with a molecular weight measurement range of $10^2 – 5 \times 10^3$ g.mol^{-1}, HR2 with a molecular weight measurement range of $5 \times 10^2 - 2 \times 10^4$ g.mol^{-1} and HR4 with a molecular weight measurement range of $5 \times 10^3 - 6 \times 10^5$ g.mol^{-1}) and a guard column was used. The columns

were heated to 40 °C during the analysis. The molecular weights were determined by calibration with linear narrow molecular weight distribution PS standards (PSS Polymer Standards Service GmbH, molecular weights ranging from 682 g.mol^{-1} to 2,520,000 g.mol^{-1}) and the GPC was equipped with a differential refractive index (RI 2414) detector. To obtain a more accurate estimation of the number-average molecular weights of the My-based polymers, the P(My) contribution to $M_{n,GPC}$ was converted using the appropriate Mark-Houwink-Sakurada (MHS) coefficients (MHS parameters determined at 40 °C with THF eluent for PS[59]: $K_{PS} = 15.8 \times 10^{-5}$ dL.g^{-1} and $\alpha_{PS} = 0.706$; MHS parameters determined at 30 °C with THF eluent for 1,4-P(My)[60], $K_{P(My)} = 7.46 \times 10^{-5}$ dL.g^{-1} and $\alpha_{P(My)} = 0.772$). Therefore, Every M_n value reported in the Results & Discussion section was calculated using the following formula: $M_n = F_{My} \times M_{n,MHS} + F_S \times M_{n,GPC}$ where F_{My} and F_S are the respective molar fraction of My and S in the final polymer and $M_{n,MHS} = [(K_{PS}/K_{P(My)}) \times M_{n,gpc}{}^{\alpha PS1}]^{(1/(\alpha P(My)+1))}$ using the Mark-Houwink relationship[61].

Thermogravimetric analysis (TGA) was carried out using Q500TM from TA Instruments under nitrogen flow at a ramp rate of 10 °C.min^{-1}. Samples were heated in aluminum pans. This technique allowed the decomposition temperature (T_d) to be determined. Differential scanning calorimetry (DSC, Q2000TM from TA Instruments) was also performed under nitrogen atmosphere in order to measure the glass transition temperatures (T_gs) of P(My), P(My-b-S) and P(My-$stat$-S) polymers. Calibrations for temperature and heat flow were done using indium and benzoic acid standards respectively. The DSC was typically performed in the temperature range from – 90 °C to + 150 °C using three scans per cycle (heat/cool/heat) at a rate of 10 °C.min^{-1}. To eliminate the thermal history, glass transition temperatures were reported from the second heating run. The reported T_gs were calculated using the injection method from the change in slope observed in the DSC traces.

The stress-strain behavior of the synthesized P(My-b-S) diblock copolymers was recorded using a MTS Insight^{TM} material testing system with a 5 kN load cell at room temperature and a cross-head speed of 1 mm.min^{-1}. Dog-bone style tensile specimens (ASTM D638, *type V*, overall length = 63.5 mm, overall width = 9.53 mm) were made using a hot press (Carver hydraulic press, model #3925) at T ~ $T_{g,specimen}$ + 50 °C where $T_{g,specimen}$ refers to the specimen's higher T_g, under a mean pressure of 5000 psi. The width (3.18 ± 0.5 mm) and the thickness (1.40 ± 0.3 mm) of the narrow section of each specimen were previously measured using a digital ruler. Each test was considered finished after the complete break-up of the specimen in two distinct parts. A minimum of five specimens was tested for each P(My-b-S) diblock copolymer sample and averaged results were reported. This mechanical characterization allowed the Young's modulus, the ultimate tensile strength and the elongation at break to be determined, using TestWorks 4 software. The Young's modulus was determined as the slope of the stress-strain curve at strains of 0-0.5 %.

RESULTS AND DISCUSSION.

A) Nitroxide-mediated polymerization (NMP) of *β*-myrcene (*My*): determination of appropriate polymerization experimental conditions.

The experimental conditions of the various *My* polymerizations performed and the characterization of the resulting poly(myrcene)s P(*My*)s at the end of the experiments are summarized Table 1 and Table 2 respectively.

Table 1. Experimental conditions for *My* polymerizations for 7 h initiated by NHS-BB.

ID	[NHS-BB]$_0$ (M)	[SG1]$_0$ (M)	$r^{(a)}$	[*My*]$_0$ (M)	Solvent[b]	[Solvent]$_0$ (M)	T (°C)	M$_{n,theo}$ (kg.mol^{-1})
My-1	0.020	0	0	3.01	Toluene	4.56	110	20.5
My-2	0.014	0	0	3.04	Toluene	4.54	110	29.6
My-3	0.008	0	0	2.94	Toluene	4.53	110	50.1
My-4	0.015	0	0	3.29	1,4-dioxane	5.12	100	29.8
My-5	0.026	0	0	5.81	-	0	110	30.4
My-6	0.025	0	0	5.61	-	0	120	30.6
My-7	0.026	0	0	5.75	-	0	130	30.1
My-8	0.027	0.001	0.049	5.87	-	0	120	29.6

| *My*-9 | 0.026 | 0.003 | 0.117 | 5.80 | - | 0 | 120 | 30.4 |

a) Initial molar concentration ratio of SG1 free nitroxide to NHS-BB initiator $= r =$ $[SG1]_0$ / $[NHS-BB]_0$.

b) Solution polymerizations done in 50 wt% solvent *versus* initial masses of *My* and NHS-BB.

� **Choice of NHS-BlocBuilder (NHS-BB) as controlling alkoxyamine.**

SG1-based initiators such as BlocBuilder[TM] or NHS-BB[54] have lower activation energy and much higher dissociation rate constants (k_d) compared to TEMPO-based initiators[62]. As a result, they can be activated at lower temperatures and allow controlled polymerizations of a wider range of monomers, such as methacrylates, 1,3-dienes and styrenic monomers. However, the use of additional SG1 nitroxide is needed to further reduce the reaction rate and produce well-defined polymers when polymerizing non-styrenic monomers initiated by BlocBuilder[TM] [50,52,63,64]. In comparison, the higher dissociation rate (~ 15 times) and slightly lower activation energy (~ 0.9 times) of NHS-BB, both measured at 120 °C in *tert*-butyl benzene, lead to rapid initiation and quick release of the SG1 rate moderator[54]. Such intrinsic features permit polymerizations to be done without any added free nitroxide at the onset of the polymerization. The NHS-BB was thus used to effectively control the homopolymerization of isoprene in bulk at 115 °C ($Đ \leq 1.15$ and $M_n = 2.4$ kg.mol^{-1} after 16 h)[53] and styrene (S) in bulk at 120 °C ($Đ \leq 1.35$ and $M_n = 21.2$ kg.mol^{-1} after 150 min)[54] without aid of additional SG1 nitroxide. Accordingly,

the NHS-functionalized alkoxyamine is predicted to be effective in obtaining well-defined P(*My*) without additional SG1 free radical.

Table 2. Molecular characterization, kinetic data and selectivity of P(*My*) synthesized for 7 h with NHS-BB.

ID	X_{My}[a]	M_n[b] (M)	$Đ$[b]	k_pK[c] (10^5 s^{-1})	1,4-content[d] (%)	*Cis*-1,4-content[e] (%)	1,2-content[d] (%)
My-1	0.56	7.5	1.35	1.9 ± 0.4	89.7	72.6	7.4
My-2	0.43	12.8	1.58	2.5 ± 0.5	87.6	-[g]	8.6
My-3	0.83	9.6	1.43	1.2 ± 0.9	81.2	66.8	11.2
My-4	0.40	8.6	1.32	1.4 ± 0.8	90.9	-[g]	4.0
My-5	0.41	8.2	1.19	1.6 ± 0.4	-[g]	-[g]	-[g]
My-6	0.66	14.9	1.26	4.3 ± 0.7	80.3	88.7	9.3
My-7	0.45	3.8	1.27	1.2 ± 0.6	82.4	-[g]	9.2
My-8	0.60	12.9	1.30	0.2 ± 0.03[f]	83.2	73.2	9.4

| My-9 | 0.80 | 13.4 | 1.46 | $0.3 \pm 0.06^{(f)}$ | 82.1 | 81.5 | 9.7 |

---

a) My conversion (X_{My}) determined gravimetrically and via ^{1}H NMR (average value).

b) M_n and M_w determined by GPC calibrated with PS standards in tetrahydrofuran (THF) at 40 °C and converted to P(My) using MHS constants.

c) k_pK corresponding to the product of the propagation rate constant k_p and the equilibrium constant K derived from the slopes $k_p[P^\bullet]$ ([$P^\bullet$] = concentration of propagating macro-radicals) taken from the semi-logarithmic kinetic plots of $ln((1-X_{My})^{-1})$ *versus* time in the linear region from 0 min to 120 min (squared linear regression coefficient = $R^2 \geq 0.95$). k_pK's estimated from $k_p[P^\bullet]$ and $r = [SG1]_0 / [NHS\text{-}BB]_0$ (Equation 6). Error bars derived from the standard errors in the slope from the linear fits of $ln((1-X_{My})^{-1})$ *versus* time.

d) Regioselectivity determined by ^{1}H NMR in CDCl$_3$. 3,4-content% not mentioned and calculated as follows: 3,4-content% = 100 – 1,4-content% – 1,2-content%.

e) Stereoselectivity determined by ^{13}C NMR in CDCl$_3$. *trans*-1,4-content% not mentioned and calculated as follows: *trans*-1,4-content% = 100 − *cis*-1,4-content%.

f) $k_p[P^\bullet] = (3.2 \pm 0.6) \times 10^{-5}$ s^{-1} for My-8 ; $k_p[P^\bullet] = (2.6 \pm 0.5) \times 10^{-5}$ s^{-1} for My-9.

g) ^{1}H and ^{13}C NMR peaks not clearly detectable.

◘ Kinetic order and apparent rate constant of *My* polymerization by NMP.

The semi-logarithmic kinetic plots of $ln((1-X_{My})^{-1})$ (X_{My} = *My* conversion) *versus* time are illustrated in Figure 2. All *My* polymerizations obeyed first order kinetics as described by Equation 4 and generated good fits to linear kinetic plots until 300 min polymerization. A loss of linearity was apparent at $X_{My} > 0.3$.

$$ln([M]_0 / [M]_t) = ln([M]_0 / ([M]_0(1-X_{My}))) = k_p \times [P^\bullet] \times time \quad (4)$$

In Equation 4, $[M]_0$ and $[M]_t$ are concentrations of monomer at time zero and a subsequent later time t, respectively, k_p is the propagation rate constant and $[P^\bullet]$ is the concentration of propagating macro-radicals. It can be first noted that almost every trend line fitted to data at the early stages of the polymerization has a positive y-intercept, suggesting the presence of polymers at the commencement of the reaction. This can be explained by the arbitrary $t = 0$ min chosen when T = 100 °C, which is relatively high compared to the NHS-BB decomposition temperature < 70 °C. For every experiment, the straight kinetic trend at $X_{My} < 0.3$ revealed a steady $[P^\bullet]$ established by balancing the rates of activation and deactivation via the SG1 free nitroxide mediator. This illustrates thereby the expected persistent radical effect (PRE)[22] based on the dynamic equilibrium between low $[P^\bullet]$ chains and a predominant amount of dormant chains. However, deviations from the linear trends are observed after the initial stages of the polymerizations, especially when a solvent was used (*My*-1, *My*-2 and *My*-3 in Figure 2.a and *My*-4 in Figure 2.b). This is explained by a change in the concentration of active propagating species $[P^\bullet]$[22]. A downward curvature, as clearly observed for experiment *My*-2 after 200 min ($X_{My} > 0.3$), suggests a decrease in $[P^\bullet]$ which may be caused by non-reversible termination reactions resulting in an increase of the concentration of the persistent radical. On the other hand,

an upward curvature, as seen for experiments *My*-1, *My*-2 and *My*-4, suggests an increase of [P•]

which may be caused by a slower initiation. This latter assumption would suggest that NHS-

BB's dissociation rate constant is slightly lower in toluene and 1,4-dioxane than in bulk. In any

case, these significant kinetic deviations starting even at moderate conversions ($X_{My} \sim 30$ %)

suggest that other undesirable processes occurred. The thermal self-initiation of *My*[75] and its

relatively low purity level (≤ 10 mol% of impurities including limonene and isomers and dimers

of My among others) might change the persistent radical concentration as well.

The slopes, calculated from four to five sample points taken in the linear region, from the

kinetic plots reveal the apparent rate constant in terms of the product of k_p with [P•], k_p[P•]. For

the systems studied here, the k_p[P•] values were all obtained during the early stages of the

polymerization, where the number-average molecular weight (M_n) increased linearly with

conversion (first 120 min of the reaction). From these values, k_pK can be estimated from

Equation 5 and Equation 6, where K is the equilibrium constant, [SG1•] is the concentration of

free nitroxide ([SG1•] = [SG1•]$_0$ is assumed in the early stages of the polymerization due to a

high initial SG1 concentration), [P-SG1] is the concentration of dormant alkoxyamine terminated

species which is assumed to be equal to the initial concentration of NHS-BB, [NHS-BB]$_0$

(generally the case in the early stages of the polymerization) and *r* is the ratio of the initial molar

concentration of SG1 free nitroxide to NHS-BB, [SG1]$_0$/[NHS-BB]$_0$.

$$K = ([P•] \times [SG1•]) / [P\text{-}SG1] \quad (5)$$

$$k_p K \cong (k_p \times [P•] \times [SG1•]_0) / [NHS\text{-}BB]_0 = k_p \times [P•] \times r \quad (6)$$

Table 2 summarizes the experimental k_pK values for the various polymerizations led.

Without additional SG1, all k_pK values are in the same order of magnitude, namely 10^{-5} s^{-1},

regardless $M_{n,theo}$ from 20 to 50 kg.mol^{-1}(DP = $[My]_0$ / $[NHS-BB]_0$ from 147 to 367), the reaction medium (in bulk or in solution) and the temperature (110 to 130 °C). When adding additional SG1 free nitroxide in the feed (*My*-8 and *My*-9), the polymerization has, by contrast, a k_pK about an order of magnitude lower (10^{-6} s^{-1}). It was expected since SG1 free radical acts as a rate moderator, slowing the reaction down[65]. However, a clear increase of the polymerization rate at the final stages of the polymerization was observed for the experiment *My*-9 with 11.7 mol% of additional SG1 relative to NHS-BB. This may be explained by a slower initiation process in the presence of a significant amount of SG1 free nitroxide, giving rise then to a higher $[P^•]$. Interestingly, induction periods may be apparent for some polymerizations such as experiment *My*-3. Indeed, at the beginning of this reaction ($t <$ 100 min), very low X_{My}s, almost plateauing, were observed. This can presumably be explained by the role of the SG1 nitroxide trapping the radicals generated at the early stages of the reaction until SG1 reached its equilibrium concentration with the dormant species. At this point, the induction time is terminated and followed by the controlled NMP (at $t >$ 100 min for experiment *My*-3, X_{My}s increased linearly with time as initially expected). k_pK values corresponding to NMP-based polymerization of isoprene in bulk at 115°C without additional SG1 are in the same range, from 0.4 to 1.4 x 10^{-5} s^{-1} [53]. These relatively slow NMP-based polymerizations of 1,3-diene monomers compared to styrenic and methacrylate monomers, which exhibit higher k_p[44,66-68], was previously noted by Hawker et al regarding the NMP of isoprene and butadiene initiated by a TIPNO-based initiator[41].
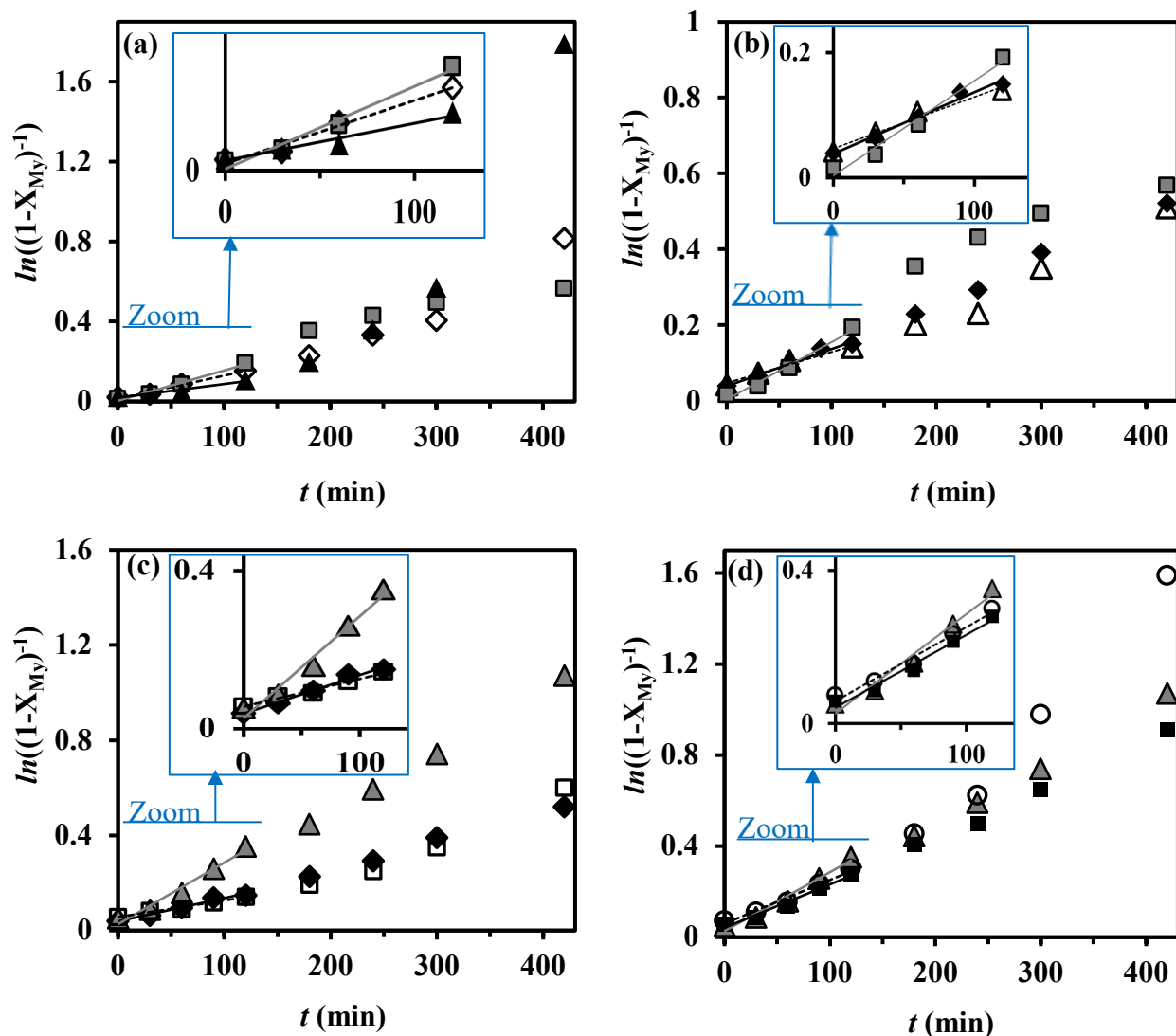
Figure 2. Semi-logarithmic kinetic plots of $ln((1-X_{My})^{-1})$ ($X_{My} = My$ conversion) *versus* polymerization time t for My polymerizations initiated by NHS-BB. **a) Influence of $M_{n,theo}$:** My-1 with $M_{n,theo} = 20.5$ kg.mol^{-1} (◊), My-2 with $M_{n,theo} = 29.6$ kg.mol^{-1} (■) and My-3 with $M_{n,theo} = 50.1$ kg.mol^{-1} (▲); **b) Influence of the reaction medium:** My-2 in toluene (■), My-4 in 1,4-dioxane (Δ) and My-5 in bulk (♦); **c) Influence of temperature:** My-5 at 110 °C (♦), My-6 at 120 °C (▲) and My-7 at 130 °C (□); **d) Influence of additional SG1:** My-6 with no additional SG1 (▲), My-8 with [SG1]$_0$ / [NHS-BB]$_0$ = 0.049 (■) and My-9 with [SG1]$_0$ / [NHS-BB]$_0$ = 0.117 (○). The straight lines indicate linear fits to the experimental data during the initial stages of the polymerization (0 to 120 min). All experimental ID and characterization of experiments are listed in Table 1 and Table 2.

◘ Influence of alkoxyamine concentration.

Attention was first paid to the theoretical number-average molecular weight ($M_{n,theo}$ = $M_{My} \times$ DP) in order to know if high molecular weight P(My) samples could be achieved by simply increasing the monomer/initiator initial molar ratio. Therefore, various amounts of NHS-BB alkoxyamine were used to prepare P(My)s by heating My at 110 °C for 7 h in 50 wt% toluene, allowing to target three different $M_{n,theo}$ at quantitative conversion (My-1, My-2 and My-3 in Table 1). P(My)s with M_n ranging from 7.5 to 12.8 kg.mol^{-1} and dispersities of 1.35-1.68 (Table 2) were synthesized. M_n were on average 87 %, 83 % and 51 % of $M_{n,theo}$ during the polymerizations (M_n/$M_{n,theo}$ average values from 0 to 7 h) as regards the experiments My-1, My-2 and My-3 respectively (Figure 3.a). Accordingly, deviations from the theoretical molar masses are higher with increasing target $M_{n,theo}$. Besides, the lowest Đ were obtained when targeting the lowest $M_{n,theo}$ (Đ of 1.14-1.35, Figure 3.a) confirming that irreversible termination reactions and/or some chain-transfer reactions[69] to My or P(My) or toluene solvent are more prevalent as $M_{n,theo}$ increasing, generating the likely loss of control. In the ideal case of a controlled/living radical polymerization, fast initiation as compared to propagation and fast exchange between active (P• in low concentration) and dormant species (P-SG1 in our situation) allow all chains to begin to grow at the same time and the reaction to be free of irreversible termination and transfer reactions. This results in a linear increase of M_n with X_{My} while Đ stays narrow (< 1.3).

The rate of polymerization was almost unaffected with the increase of the NHS-BB concentration, k_pK staying around 2.0 10^{-5} s^{-1}. An increase of the k_pK with lower $M_{n,theo}$ could have been expected as those polymerizations may have a reduced probability of irreversible termination reactions compared to polymerizations with higher target M_n[63]. Moreover, in such a situation with a lower $M_{n,theo}$, the equilibrium may not strongly favour the alkoxyamine such that

the instantaneous chain radical concentration is not low enough to avoid bimolecular termination reactions. Accordingly, bimolecular termination events may be more apparent, resulting in an increase of the overall polymerization rate until the steady state predicted by the PRE is reached. Harrisson and al reported[53] an increase of the rate of isoprene polymerization in a nonlinear manner with the concentration of BlocBuilder[TM], the rate of reaction being proportional to [BlocBuilder[TM]]$^{0.42}$.

A target number-average molecular weight of 30 kg.mol^{-1} (DP = $[My]_0$ / $[NHS-BB]_0$ = 220) is thereafter chosen since it allowed achieving relatively high average chain length P(My) with a decent degree of control.
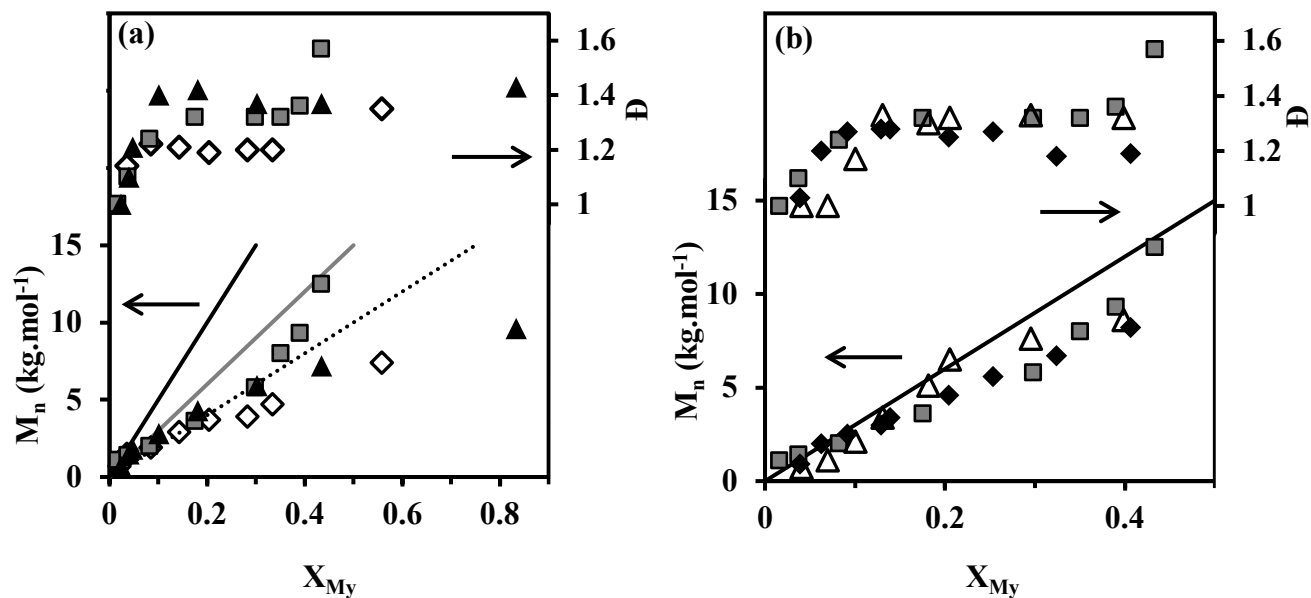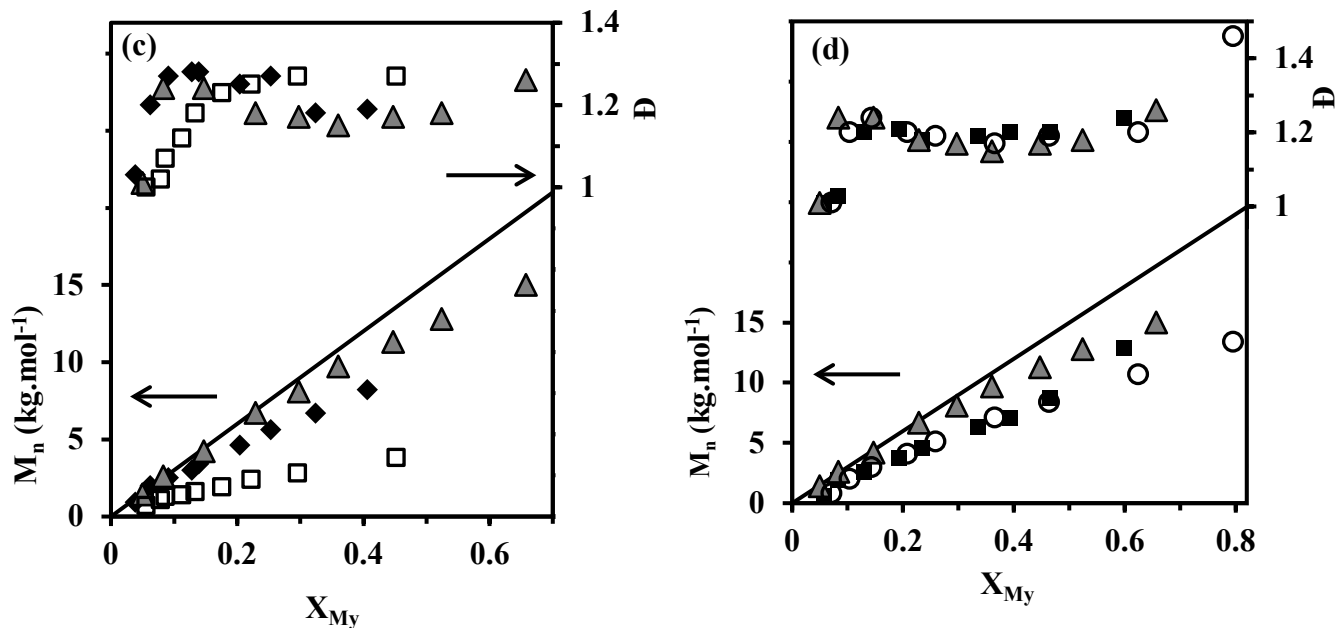
Figure 3. M_n determined by GPC relative to PS standards in THF and corrected with appropriate MHS coefficients and Đ *versus* conversion for the various *My* polymerizations initiated by NHS-BB. **a) Influence of $M_{n,theo}$:** *My*-1 with $M_{n,theo}$ = 20.5 kg.mol^{-1} (◊), *My*-2 with $M_{n,theo}$ = 29.6 kg.mol^{-1} (■) and *My*-3 with $M_{n,theo}$ = 50.1 kg.mol^{-1} (▲); **b) Influence of the reaction medium:** *My*-2 in toluene (■), *My*-4 in 1,4-dioxane (∆) and *My*-5 in bulk (♦); **c) Influence of temperature:** *My*-5 at 110 °C (♦), *My*-6 at 120 °C (▲) and *My*-7 at 130 °C (□); **d) Influence of additional SG1:** *My*-6 with no additional SG1 (▲), *My*-8 with $[SG1]_0 / [NHS-BB]_0 = 0.049$ (■) and *My*-9 with $[SG1]_0 / [NHS-BB]_0 = 0.117$ (○). The straight lines indicate the theoretical M_n ($M_{n,theo}$) *versus* conversion based on the monomer to initiator ratio for the particular experiment. All experimental ID and characterization of experiments are listed in Table 1 and Table 2.

Influence of the reaction medium.

The presence of a solvent, due to its polarity and its viscosity for instance, can induce drastic changes for both k_d[70] and k_c (rate of recombination)[71] of the initiator. A loss of control can be generated by chain-transfer reactions to the solvent as highlighted by Charleux and coworkers for the NMP of acrylic acid in 1,4-dioxane[64,72]. On the other hand, the solvent can also improve the control of the NMP. Harrisson and al reported better control of isoprene polymerization by SG1-based NMP when using 1,4-dioxane and pyridine instead of bulk, due to a disruption of intramolecular hydrogen bonding within the alkoxyamine initiator and stabilization of the SG1 free nitroxide[73]. Accordingly, it is of interest to determine the influence of the reaction medium, which may play a significant role on the NMP of *My*.

The polymerization of *My*, mediated by NHS-BB, was carried out at 110 °C in toluene (50 wt%) and in bulk, and at 100 °C in 1,4-dioxane (50 wt%) due to its lower boiling point ($T_{b,1,4\text{-dioxane}} = 101$ °C), while keeping $M_{n,theo}$ constant around 30 kg.mol^{-1} (*My*-2, *My*-5 and *My*-4 respectively in Table 1). No change in the overall rate of polymerization was observed as k_pK values were not significantly different and the final conversion was around 0.4, regardless of the reaction medium (Table 2). The molecular weights for each experiment followed the same trend with a linear increase of up to 20 % conversion and a slight plateau at higher conversions (Figure 3.b) indicating presumably the occurrence of irreversible termination reactions. Interestingly, narrower molecular weight distributions were obtained when performing *My* polymerization in bulk (Đ ≤ 1.27, Figure 3.b). The slightly higher Đ obtained for the two solution polymerizations might be explained by the extra contribution of chain-transfer side reactions to toluene and 1,4-dioxane.

Accordingly, *My* polymerization in bulk gave satisfactory results in terms of control compared to that in solution using 1,4-dioxane and toluene. Bulk polymerization of *My* was thus applied for further studies.

◘ Determination of the appropriate polymerization temperature.

A third series of *My* NMPs was undertaken, varying only one experimental parameter, namely the reaction temperature, ranging from 110 °C to 130 °C (*My*-5, *My*-6 and *My*-7 in Table 1). This was made possible through the low volatility of this monoterpene ($T_{b,My} = 167$ °C). Increasing the temperature from 110 °C to 120 °C more than doubled the k_pK value with significantly greater conversions (~ 1.7 times on average) during the experiment (Table 2). Therefore, an increase in the overall rate of polymerization, as expected by the Arrhenius equation[74], was observed. Furthermore, contrary to what one might think, this was not accompanied by a loss of control over the polymerization. Indeed, M_n increased linearly with X_{My} with slight discrepancies at the final stages. M_n values were on average 90 % of the theoretical ones while Đ remained below 1.3 (Figure 3.c). Unexpectedly, polymerization at 130 °C was not faster than that at 120 °C. Its overall rate of polymerization was very close to that of the polymerization performed at 110 °C (Figure 2.c). Besides, despite low Đ ≤ 1.3, significant deviations from the predicted line were observed regarding the average molecular weights (Figure 3.c). This marked loss of control occurring from the early stages of the experiment may be due to irreversible termination reactions, which were becoming more frequent at higher temperature.

Consequently, a reaction temperature of 120 °C (experiment My-6) was deemed satisfactory since it provides a polymerization at least as controlled as at 110 °C combined with a higher overall rate of reaction. Similarly, 115 °C was the optimized reaction temperature of the SG1-based NMP of isoprene for a control polymerization at an acceptable rate of reaction[53]. The GPC traces for My-6 are given in Figure 4 and exhibit a monomodal shift of relatively narrow peaks taken at different points in the polymerization. A second and minor population of longer P(My) chains can be generally detected at the early stages of the polymerization as observed at t = 1 h. This higher M_n peak, generally observed for almost every My polymerization led, appeared at the commencement of the reaction ($t < 60$ min), remained constant (no clear shift to lower elution volumes) to become not detectable by GPC at the last stages of the experiment. A negligible fraction of high M_n P(My) was therefore obtained at the end of the reactions compared to the amount of well-controlled polydiene chains. This may be due to My autoinitiation increasing the amount of propagating radicals that would not necessarily be reversibly terminated by the SG1 and therefore would not be controlled (deviation from the initial stoichiometry with [P$^•$] > [SG1$^•$]). Although autopolymerization should be moderated by the equilibrium established by the PRE, My autopolymerization is likely significantly faster than My NMP making the mediation by SG1 more complicated. It should be noted that the presence of a high M_n peak was likewise observed at the early stages of most of the My polymerizations performed such as experiment My-10-S (Figure 5.a) and experiment My/S-50 at 1 h (Figure 8). Lastly, a GPC measurement of commercial My used (grade $\geq$ 90 %, stored at 4-5 ^{0}C to prevent early polymerization) indicated the absence of any polymers. The assumption that high M_n P(My) could be already present before polymerization does not appear relevant, autopolymerization

being inhibited at low T and impurities consisting mainly in monomers and dimers. Since the 1950s, *My* is known to polymerize spontaneously at elevated temperature as other conjugated dienes whereas its loss by autopolymerization at Troom was estimated to one third after three months without inhibitor[75].
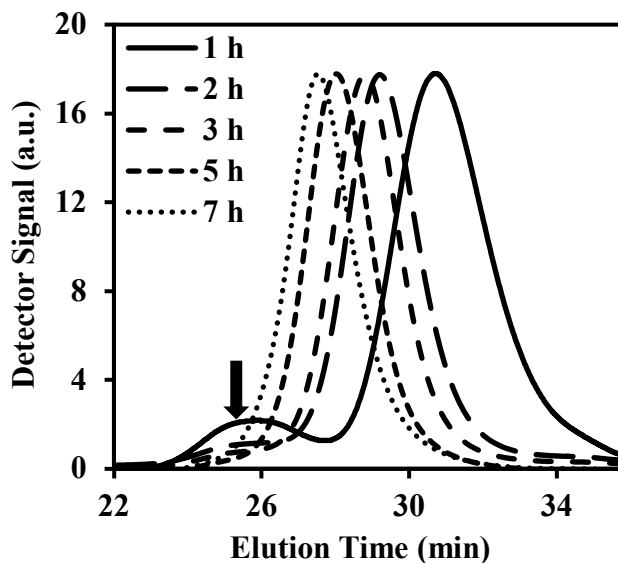
Figure 4. Normalized GPC traces of P(*My*) initiated by NHS-BB at 120 °C in bulk targeting $M_{n,theo} = 30$ kg.mol^{-1} at quantitative conversion (experiment *My*-6). The arrow indicates the peak/shoulder observed at $t = 1$ h corresponding to a minor fraction of high molecular weight P(*My*) ($M_n = 45.3$ kg.mol^{-1}, Đ = 1.28) presumably due to *My* autoinitiation.

�« **Effects of additional SG1 free nitroxide.**

The effectiveness of additional SG1 over the control of non-styrenic monomer polymerizations initiated by the BlocBuilder[TM] initiator was demonstrated. For instance, the control of *tert*-butyl acrylate polymerization was improved by introducing 5-6 % of free nitroxide relative to the BlocBuilder[TM] initiator, reducing both the overall rate of reaction and the Đ values[76]. In order to know if such a strategy could be efficient for the system *My*/NHS-BB, two extra experiments were undertaken: *My*-8 and *My*-9 with respectively 4.9 % and 11.7 % of additional SG1 mediator relative to NHS-BB and implemented under the optimized reaction conditions, namely in bulk at 120 °C targeting 30 kg.mol^{-1} at X_{My} = 100 % (Table 1). The results were compared with experiment *My*-6 where no additional SG1 was used. Adding about 5 % of additional SG1 relative to NHS-BB in the feed did not affect the polymerization of *My*, exhibiting nearly identical overall rate of reaction (Figure 2.d) and M_n and Đ values over time not significantly different (Figure 3.d). More surprising, a loss of control seems to be apparent in the late stages of the polymerization (t > 240 min, X_{My} > 0.46) when around 12 % of SG1 free radical was added initially. A loss of linearity was highlighted in the $ln((1-X_{My})^{-1})$ *versus* time plot (Figure 2.d) combined with greater deviations of the experimental molar masses from the theoretical ones (Figure 3.d). It might be explained by a higher rate of irreversible termination by *β*-hydrogen chain-transfer (disproportionation) to SG1, as shown by McHale and coworkers for the system SG1/MMA (methyl methacrylate) when using large excesses of nitroxide[77]. In our case, the percentage of free nitroxide was relatively low and a further analysis would be necessary to clearly identify the possible main chain-end forming event occurring. Another assumption explaining these results for experiment *My*-9 with the highest r = 0.117 may be the contribution to extra SG1 nitroxide to high M_n propagating macroradicals resulted from self-initiation of *My*. In that case, higher deviations of the measured M_n from $M_{n,theo}$ can be expected

as well without however bringing about a loss of control (linear trend of M_n versus X_{My} and Đ <

1.3 except at the end of the reaction, Figure 3.d).

◘ **Microstructural features of NMP-based P(*My*).**

My is expected to yield P(*My*) polymer with a variety of structural units. Such a

substituted diene system can produce units of 1,2-, 3,4-, 1,4-*cis* and 1,4-*trans*. 1,2-, 3,4- and 1,4-

isomers were detected by ^{1}H NMR whereas the signature peaks for 1,4-*cis* and 1,4-*trans* motifs

were obtained from ^{13}C NMR spectra (see Supporting Information for the spectral assignments

of ^{1}H NMR and ^{13}C NMR from typical experiments, Figures S2 and S3). The analyses were in

good accordance with the literature[21,58]. The proportions of these four different types of

microstructure at the end of each polymerization are given in Table 2. It can be concluded that

the NMP of *My* initiated by NHS-BB affords a P(*My*) that is 1,4-regular (80 to 90 %) with 1,2-

(5 to 10 %) and 3,4-defects (5 to 10 %). This is in agreement with the predominant 1,4-

microstructure (96 %) of P(*My*) synthesized by RAFT with 2-ethyl-sulfanylthiocarbonylsulfanyl-

propionic acid ethyl ester chain-transfer agent[36]. More generally, the 1,4-motif is typically

dominant (> 75 %) by free radical polymerization[12,13,15,16] of *My*. Similar proportions of 1,4-

addition (81 %), 1,3-addition (13 %) and 1,2-addition (6 %) were determined for the NMP in

bulk of isoprene[53]. Moreover, the NMP-based poly(terpene) exhibits a high *cis*-selectivity, higher

than 65 %. The coexistence of *cis* and *trans* isomers was qualitatively reported regarding RAFT-

based[36] and emulsion-based[16] P(*My*)s.

B) Synthesis of poly(myrcene-*block*-styrene) P(*My-b-*S) diblock copolymer

◘ Chain-extension with styrene (S) from poly(myrcene) P(*My*) macroinitiator.

The active feature of NMP-based polymers is enabled due to the nitroxide moieties capped at the chain ends. To investigate the ability of the expected SG1-terminated P(*My*) homopolymer to re-initiate a second batch of monomer, chain-extension experiments were performed using S monomer and three P(*My*) macroinitiators (*My*-10, *My*-11 and *My*-12) exhibiting different degrees of polymerization (13.2 kg.mol^{-1} < M$_n$ < 30.4 kg.mol^{-1}). The experimental conditions and results of these experiments are summarized in Table 3 and Table 4, respectively. With a fresh batch of purified styrene, P(*My*) macroinitiator was extended with a poly(styrene) PS block with M$_n$ ranging approximately from 12 to 26 kg.mol^{-1}. Đ of the diblock copolymers (1.33, 1.83, 1.50 and 1.88) were higher than that of their macroinitiator (1.18, 1.32, 1.32 and 1.38). This broadening of Đ after the chain-extensions can be due to the diffusion of the mediating SG1 radical from the propagating chain end to styrene monomer. Side reactions involving radical crossovers for NMP were reported by Hawker et al[78]. This assumption is consistent with the reactivity ratios of *My* and S determined in part C highlighting the shiftless and unprivileged addition of S towards the propagating radical --*My*˙. Besides, irreversible termination and some macroinitiator chains which were not initiated could also have contributed to the loss of control observed during these chain-extensions. The S molar composition of the synthesized P(*My-b-*S) copolymers (F$_S$), measured via ^{1}H NMR spectroscopy (^{1}H NMR spectrum of recovered P(*My-b-*S) copolymer *My*-11-Sa provided in the Supporting Information, Figure S4) varied from 27 to 62 mol%.

Table 3. Formulations of chain-extensions with purified S using various P(*My*) macroinitiatiors in 50 wt% toluene solution at 110 °C.

	Macroinitiator		Formulation of chain-extension				
ID	M_n (kg.mol^{-1})	Đ	[Macroinitiator]$_0$ (M)	[S]$_0$ (M)	[Toluene]$_0$ (M)	$M_{n,theo}$[a] (kg.mol^{-1})	t (min)
My-10-S	13.2	1.18[c]	0.006	3.442	4.812	73	300
My-11-Sa[b]	22.8	1.32	0.005	3.242	4.829	90	420
My-11-Sb[b]	22.8	1.32	0.005	3.143	4.802	88	140
My-12-S	30.4	1.38	0.004	3.026	4.809	109	120

a) $M_{n,theo}$ corresponding to the targeted number-average molecular weight of the whole P(*My-b*-S) diblock copolymer at 100% of S conversion.

b) Same P(*My*) macroinitiator used for these two experiments.

c) Tail observed at about 24 min elution time (Figure 5.a) not integrated for the measurement of the molecular weight distribution.

The GPC chromatograms of the chain-extension experiments are shown in Figure 5. For every experiment, the P(My-b-S) chain-extended block copolymer (dotted line) shifted to lower elution time compared to its P(My) macroinitiator (solid line). These marked shifts demonstrated the increase of M_n with polymerization time. Moreover, the GPC traces of the chain-extended polymers retained generally their monomodal nature, indicating a high level of chain end fidelity. For each experiment, the tails of chain-extended copolymers overlap to some degree with the associated macroinitiator traces. This tailing, partly due to the presence of "dead" chains from the macroinitiator, was slightly more apparent for the chain-extensions My-11-Sa and My-12-S where high $M_{n,theo}$ was targeted ($\geq$ 90 kg.mol^{-1}) combined, in the case of My-11-Sa, with a long reaction time. Under such conditions, irreversible terminations are more prevalent, geneirating a loss of control which can be also highlighted by the increase of Đ > 1.8 at the end of these chain-extensions.

Table 4. Molecular and mechanical characterization of diblock copolymers after chain-extension with purified S from various P(My) macroinitiatiors at 110 °C in 50 wt% toluene.

ID	X_S[a]	F_S[b]	M_n[c] (kg.mol^{-1})	Đ[c]	E[d] (MPa)	Ultimate tensile strength[d] (MPa)	Tensile elongation at break[d] (%)
My-10-S	0.34	0.62	33.7	1.33	-[e]	-[e]	-[e]
My-11-Sa	0.38	0.47	49.0	1.83	264 ± 53	0.86 ± 0.19	0.80 ± 0.15
My-11-Sb	0.22	0.39	38.5	1.50	126 ± 70	0.63 ± 0.06	1.57 ± 0.18

| *My*-12-S | 0.31 | 0.27 | 42.6 | 1.88 | 6 ± 4 | 0.37 ± 0.05 | 13.94 ± 1.63 |

a) S conversion (X_S) determined only by ^{1}H NMR spectroscopy in CDCl$_3$.

b) Molar fraction of S in the copolymer (F_S) as determined by ^{1}H NMR in CDCl$_3$.

c) M_n and M_w determined by GPC calibrated with PS standards in tetrahydrofuran (THF) at 40 °C. M_n of the P(*My*) segment corrected for each experiment using the appropriate MHS parameters.

d) Young's modulus (E), ultimate tensile strength and tensile elongation at break measured by uniaxial tensile testing via a MTS Insight^{TM} material testing system with a 5 kN load cell at room temperature and a cross-head speed of 1 mm.min^{-1}. 6, 5 and 5 specimens tested for the experiments *My*-11-Sa, *My*-11-Sb and *My*-12-S respectively. Averaged results given with the respective standard deviations.

e) Specimens too brittle to perform tensile testing.

In summary, these results confirmed the ability of NMP-based P(*My*) macroinitiator to reinitiate a new batch of styrene and polymerize in a controlled way. Slight tails were observed, likely due to a small portion of inactive macroinitiator as well as the occurrence of irreversible termination events.
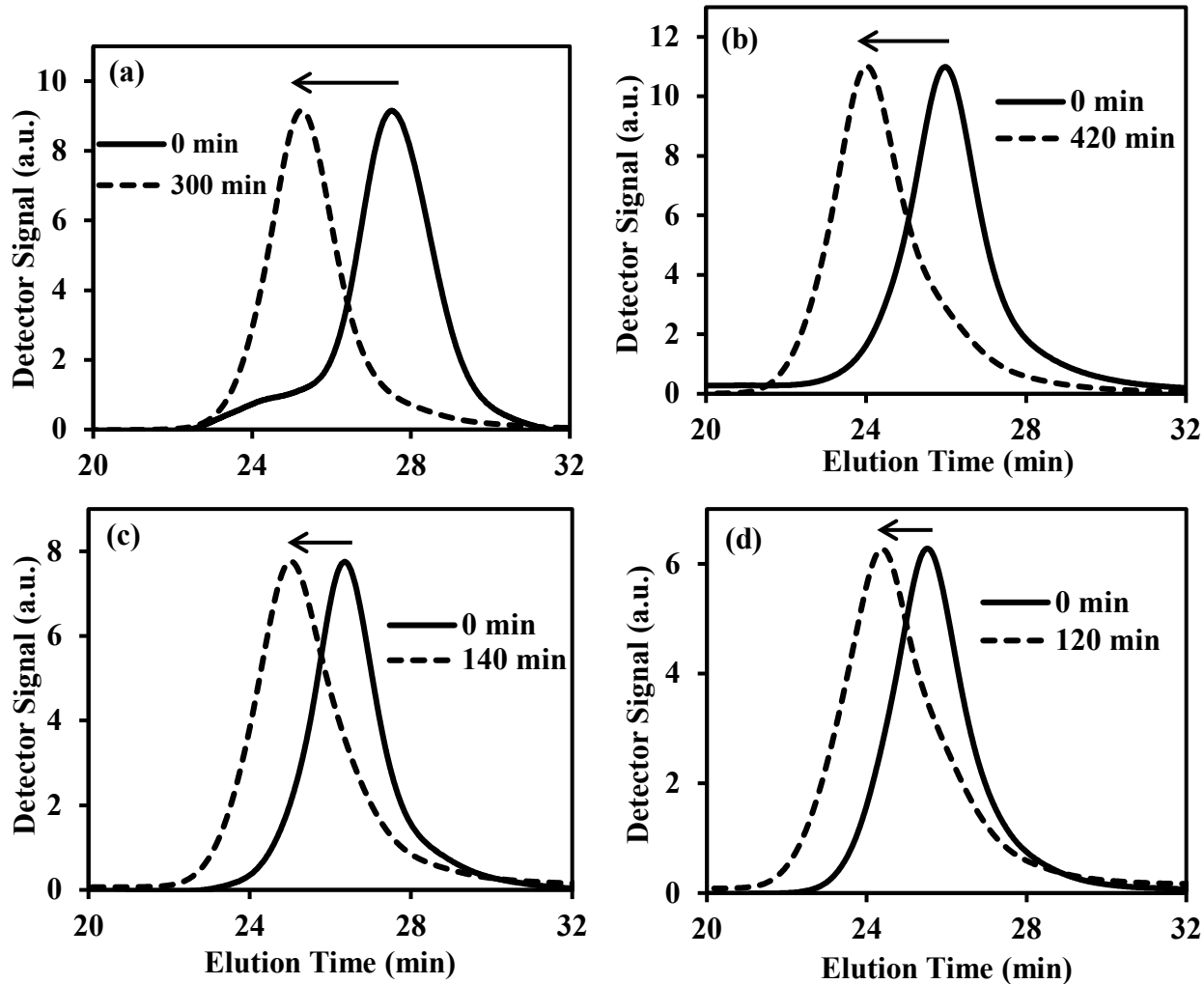
Figure 5. Normalized GPC traces for S chain-extensions from various P(*My*) macroinitiators at 110 °C in 50 wt% toluene. **a)** is the chain extension experiment *My*-10-S; **b)** is the chain extension experiment *My*-11-Sa; **c)** is the chain extension experiment *My*-11-Sb; **d)** is the chain extension experiment *My*-12-S.

◻ **Tensile properties of P(*My-b*-S) diblock copolymer.**

Uniaxial tensile testing was performed on the resulting P(*My-b*-S) diblock copolymers, with F_S = 0.27-0.62, in order to determine their mechanical behavior. Table 4 gives the tensile

properties of the various copolymers and Figure 6 illustrates the stress-strain curves of two specimens from experiments *My*-11-Sa (F_S = 0.47) and *My*-12-S (F_S = 0.27) (all stress-strain curves of the specimens from *My*-11-Sa, *My*-11-Sb and *My*-12-S samples provided in the Supporting Information, Figures S6, S7 and S8).

Regardless of the molar composition of the samples, all stress-strain curves were marked by a linear elastic region, followed by a short failure region. No plastic deformation was observed, resulting in a failure point very close to the yielding point. Every specimen, breaking after reaching their elastic limit, exhibited both brittle behavior with low ultimate tensile strength (< 1.1 MPa, Table S1 in Supporting Information) and low extensibility with poor elongation at break (< 16 %, Table S1 in Supporting Information). Materials from experiment *My*-10-S, even more fragile, fractured before performing the mechanical test. As a comparison, isoprene/styrene P(I-*b*-S) triblock copolymer having slightly higher overall M_n (68.5 kg.mol^{-1}) and F_S (0.40) exhibited thermoplastic elastomeric mechanical behavior with significant strength (tensile stress at break > 20 MPa) combined with high elongation at break (> 1000 %)[79]. Likewise, butadiene/styrene P(B-*b*-S) triblock sample exhibing M_n = 73 kg.mol^{-1} and F_S = 0.40 had largely better stress-strain properties with tensile stress at break higher than 20 MPa and elongation at break higher than 700 %[80], in comparison to the NMP-based P(*My*-*b*-S) copolymers. Such a mechanical behavior for P(I-*b*-S) and P(B-*b*-S) triblocks can be in part explained by a highly entangled polydiene matrix forming the flexible rubbery domain. P(I-*b*-S) and P(B-*b*-S) triblock copolymers mentioned above exhibited M_n for the elastomeric block ($M_{n,PI}$ = 41.1 kg.mol^{-1} and $M_{n,PB}$ = 41.2 kg.mol^{-1}) largely higher than their respective entanglement molecular weight ($M_{e,PI}$ = 4-6 kg.mol^{-1} and $M_{e,PB}$ = 2-4 kg.mol^{-1})[81], allowing the matrix phase to have a high entanglement density. By contrast, the maximum M_n of the poly(terpene) segment in

the P(*My-b*-S) copolymers was ~ 30.4 kg.mol^{-1} (experiment *My*-12-S), only slightly higher than

P(*My*) entanglement molecular weight ($M_{e,P(My)}$ = 22-31 kg.mol^{-1})[81]. Although *My*-12-S sample

may have been entangled, it is very likely that *My*-11-Sa and *My*-11-Sb samples exhibiting

shorter P(*My*) chains ($M_{n,P(My)}$ = 22.8 kg.mol^{-1}) did not form an entangled elastomeric phase.

This difference in mechanical behavior between P(*My-b*-S) diblock samples and P(I-*b*-S) / P(B-

b-S) triblock samples was presumably due to different molecular architectures as well. When the

rubbery segment (P(*My*), PI or PB) is in excess of the rigid segment (PS) so that the rubber forms

the continuous phase, the triblock copolymers have generally higher tensile strengths compared

to similar diblock copolymers[82]. The rigid segment is aggregated in both cases and both types of

block copolymers have the characteristics of a rubber containing rigid fillers. However, the

rubber phase acts like it is cross-linked in triblock polymers because both ends of each

elastomeric chain are attached to a rigid dispersed phase (entanglements are physically trapped).

In the diblock polymer, the rubber chains are attached to a rigid chain at only one end and

therefore are not cross-linked. Adhikari studied the influence of the presence of 60 wt% of P(B-

b-S) diblock chains (F_S = 0.5) to linear P(B-*b*-S) triblock copolymers (F_S = 0.5) on the

mechanical properties of this latter. Although the strain at break values were similar for both

types of structures (~ 900 %), P(B-*b*-S) triblock copolymer containing an important amount of

P(B-*b*-S) diblock chains exhibited tensile stress at break (< 15 MPa) significantly lower in

comparison to the pure P(B-*b*-S) triblock (> 30 MPa)[83]. Therefore, it can be assumed that the

poor tensile properties exhibited by the P(*My-b*-S) diblock copolymers were also due their

network architecture since only one end of the P(*My*) chains was anchored to a PS glassy

domain. The untrapped P(*My*) endblocks were thus able to relax stress by chain reptation,

reducing the elastic response of the physical network.
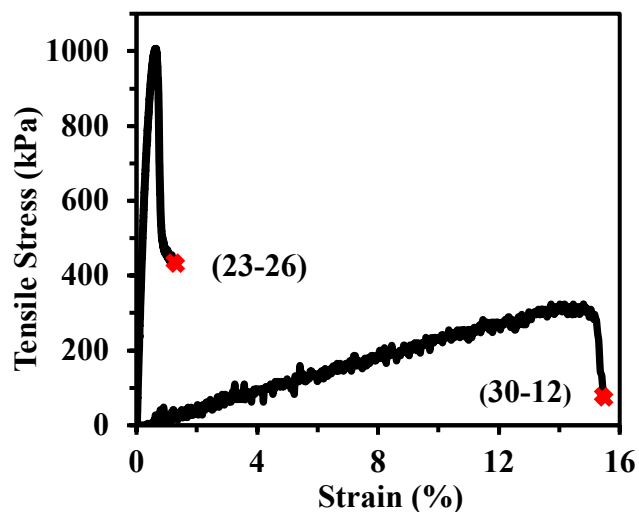
Figure 6. Tensile stress-strain curves of two P(*My-b*-S) diblock copolymer specimens from experiment *My*-11-Sa (specimen 5) with $M_{n,P(My)} = 22.8$ kg.mol^{-1} and $M_{n,PS} = 26.2$ kg.mol^{-1} (23-26) and from experiment *My*-12-S (specimen 2) with $M_{n,P(My)} = 30.4$ kg.mol^{-1} and $M_{n,PS} = 12.2$ kg.mol^{-1} (30-12) at room temperature and 1 mm.min^{-1}. The red crosses denote failure points.

The modulus of elasticity (E), also known as Young's modulus, is defined by the slope of the linear elastic region of the stress-strain curve[84]. As expected, synthesized P(*My-b*-S) Young's modulus, ranging from 10^1 to 10^2 MPa in order of magnitude, is between P(*My*) Young's modulus ($E_{P(My)} \sim 10^{-3}$ MPa)[16] and PS Young's modulus ($E_{PS} \sim 10^3$ MPa)[85]. This elastic modulus range measured experimentally is in agreement with that of P(I-*b*-S) triblock copolymers (1 MPa < E < 900 MPa) prepared by anionic polymerization and exhibiting an overall M_n of about 100

kg.mol^{-1} and F_S = 0.19-0.58[86]. Furthermore, it is of interest to note that tensile testing for P(*My-b*-S) samples showed ultimate tensile strength values ranging from 0.4 to 0.9 MPa and elongations at break ranging from 1 to 14 %. This suggests that mechanical properties of P(*My-b*-S) block copolymers can be readily tuned based on molar composition. The greater the molar fraction of *My*, the higher the elongation at break and the lower the Young's modulus and the ultimate tensile strength as previously reported by Bolton and al for *β*-myrcene/*α*-methyl-*p*-methylstyrene triblock copolymers[21].

C) *My*/S statistical copolymerization by NMP

My/S mixtures, with initial S molar feed compositions $f_{S,0}$ = 0.10-0.94 were copolymerized by NMP in bulk using NHS-BB as initiator and a target molecular weight at full conversion of $M_{n,theo}$ = 30 kg.mol^{-1}. Every experiment was performed at 110 °C in order to avoid the autoinitiation of S which is negligible below 120 °C[87]. However, autoinitiation pathways involving dimerization of S and *My* might occur at 110 °C. Order-of-magnitude estimate of the rate constant for the dimerization of S and *My* could be made by inhibition experiments for example. It would allow knowing if any thermal radical generation in the spontaneous *My*/S copolymerization (initiation step) occurs. Table 5 indicates the formulations of the various *My*/S copolymerizations.

Table 5. My/S copolymerization formulations for various compositions at 110 °C in bulk initiated by NHS-BB and targeting $M_{n,theo} = 30$ kg.mol^{-1} at X = 1.0.

ID[a]	[NHS-BB]$_0$ (M)	[My]$_0$ (M)	[S]$_0$ (M)	$f_{S,0}$	t (min)
My/S-0	0.026	5.83	0	0	420
My/S-10	0.027	5.44	0.59	0.10	420
My/S-20	0.027	5.00	1.31	0.21	420
My/S-30	0.025	4.54	2.03	0.31	420
My/S-40	0.027	4.04	2.66	0.40	420
My/S-45	0.027	3.77	3.11	0.45	420
My/S-50	0.028	3.50	3.59	0.51	420
My/S-60	0.029	2.91	4.32	0.60	420
My/S-70	0.028	2.28	5.18	0.69	420

My/S-80	0.029	1.59	6.47	0.80	360[b]
My/S-90	0.030	0.83	7.02	0.89	400
My/S-95	0.031	0.43	7.35	0.94	180[b]
My/S-100	0.030	0	8.72	1	150[b]

a) Experimental identification (ID) given by *My*/S-XX where the number abbreviation XX refers to the rounded % initial molar fraction of S in the mixture ($f_{S,0}$).

b) Experiments stopped before 420 min due to a highly viscous reaction medium.

◘ Effect of feed composition on copolymer composition.

An investigation of how feed composition controls the copolymer composition was first performed. The compositions of the copolymers (F_S and $F_{My} = 1 - F_S$, Table 6 for the final compositions) were determined by ^{1}H NMR (see experimental section for full information). The terminal model[88] was used herein, postulating that the chemical reactivity of a propagating chain depended only on the chemical nature of the active monomer at the chain end.

Table 6. Molecular characterization at the end of the experiments and kinetic data of P(*My-stat*-S) copolymers at 110 °C in bulk initiated by NHS-BB and targeting $M_{n,theo} = 30$ kg.mol^{-1} at X = 1.0.

ID	F_S[a]	X_{My}[b]	X_S[b]	X_{NMR}[b]	M_n[c] (kg.mol⁻¹)	$Đ$[c]	$\langle k_p \rangle \langle K \rangle$[d] ($10^5$ s⁻¹)
My/S-0	0	0.40	0	0.40	8.2	1.19	1.6 ± 0.3
My/S-10	0.08	0.47	0.39	0.46	12.6	1.25	2.2 ± 0.1
My/S-20	0.15	0.44	0.33	0.42	10.0	1.26	1.5 ± 0.3
My/S-30	0.28	0.41	0.37	0.40	8.4	1.24	1.2 ± 0.3
My/S-40	0.38	0.50	0.45	0.48	13.7	1.25	1.8 ± 0.2
My/S-45	0.34	0.40	0.28	0.35	10.0	1.33	1.3 ± 0.2
My/S-50	0.48	0.50	0.45	0.47	11.7	1.19	1.7 ± 0.4
My/S-60	0.31	0.38	0.31	0.34	9.8	1.36	1.1 ± 0.6
My/S-70	0.45	0.54	0.45	0.48	13.9	1.24	1.2 ± 0.3
My/S-80	0.66	0.89	0.95	0.94	13.8	1.33	2.5 ± 0.6
My/S-90	0.83	0.84	0.78	0.79	19.8	1.31	2.0 ± 0.7

My/S-95	0.96	0.81	0.89	0.89	11.0	1.37	4.1 ± 1.1
My/S-100	1	0	0.88	0.88	15.6	1.20	7.5 ± 0.8

a) See notation b) in Table 4.

b) Individual monomer conversions X_{My} and X_S determined by ^{1}H NMR. Average monomer conversion $X_{NMR} = \mathbf{X_{My}f_{My,0}} + \mathbf{X_S f_{S,0}}$ (further details in the experimental section).

c) M_n and M_w determined by GPC calibrated with PS standards in THF at 40 °C. Appropriate MHS coefficients and $F_{My} = 1 - F_S$ used to convert molecular weights based on PS to the fraction of *My* incorporated in the P(*My-stat*-S) copolymer.

d) See notation c) in Table 2 ($R^2 \geq 0.94$).

Extraction of the reactivity ratios was done by linearization of the Mayo-Lewis equation[89] (eg. the Fineman-Ross (FR) approach[90]) and by the Kelen-Tüdös (KT) approach[91] (equations and experimental data used to determine the reactivity ratios can be found in the Supporting Information, pages S10 and S11 (Table S2) respectively). FR and KT plots are shown in Figures 7.a and 7.b respectively and yielded $r_{My} = 1.88 \pm 0.12$ and $r_S = 0.25 \pm 0.04$ ($r_{My} \times r_S = 0.47 \pm 0.11$) via the FR method and $r_{My} = 2.19 \pm 0.07$ and $r_S = 0.34 \pm 0.19$ ($r_{My} \times r_S = 0.74 \pm 0.41$) via

the KT method. The errors associated with the experimental data were derived from the standard errors of the slopes from FR and KT plots. Although the KT method is more reliable than the FR method, it is still a linearization. Statistically, a non-linear least-squares fit to the Mayo-Lewis equation is probably the soundest method to determine the desired parameters[92]. Therefore, the reactivity ratios were also determined using a non-linear least-squares fitting of the data. Using the reactivity ratios determined by the KT method as initial guesses, the statistical fit to the data yielded reactivity ratios $r_{My} = 2.90 \pm 1.25$ and $r_S = 0.47 \pm 0.27$ (see Supporting Information, page S10), which are consistent compared to those obtained by the other approaches. For all of the methods, $r_{My} > 1$ and $r_S < 1$, suggesting that My monomer is more reactive than S monomer toward both propagating species (--$My^\bullet$ and --$S^\bullet$). The macro-radicals had a marked preference for My and the copolymers formed instantaneously were always richer in My than S. A compositional drift was observed as indicated by the product $r_{My} \times r_S$ being less than unity. In the initial stages of the copolymerization, My was incorporated faster, producing a My-rich copolymer. When My was depleted, more S monomer was added. This specific behavior is highlighted by the difference in copolymer composition between the initial and the final stages of the reaction. For instance, the copolymer was composed of 76 mol% of My at 1 h and only of 53 mol% of My at 7 h for the experiment My/S-50 with $f_{S,0} = 0.51$ (individual My and S conversions in the course of the experiment My/S-50 provided in the Supporting Information, Figure S9). The reactivity ratios for My/S free radical copolymerization in bulk initiated by azobisisobutyronitrile (AIBN) at 65°C were also determined, $r_{My} = 1.36$ and $r_S = 0.27$, using a non-linear least-squares method[14]. Similar behaviors were observed for isoprene/styrene I/S ($r_I = 1.92$-2.02 and $r_S = 0.42$-0.54)[93,94] and butadiene/styrene B/S ($r_B = 1.35$-1.83 and $r_S = 0.37$-0.84)[95-101] free radical

copolymerizations, confirming the more reactive nature of these 1,3-diene monomers compared to S.

The Mayo-Lewis plot is depicted in Figure 7.c and shows that NMP-based P(*My-stat*-S) formed instantaneously was always richer in *My*, regardless the initial *My*/S composition, with no azeotrope observed. A similar trend curve was obtained by Trumbo although the P(*My-stat*-S)s, synthesized by free radical polymerization in bulk at 65 °C in this case, contained a higher fraction of S[14]. This is explained by a lower *My* reactivity ratio (r_{My} = 1.36)[14] in comparison to that of the SG1-based nitroxide-mediated statistical copolymerization (r_{My} ≥ 1.88). The possible temperature dependence of *My*/S copolymerization reactivity ratios may explain the difference in P(*My-stat*-S) composition for similar $f_{S,0}$ between Trumpo's copolymers made at 65 °C and NMP-based copolymers made at 110 °C.
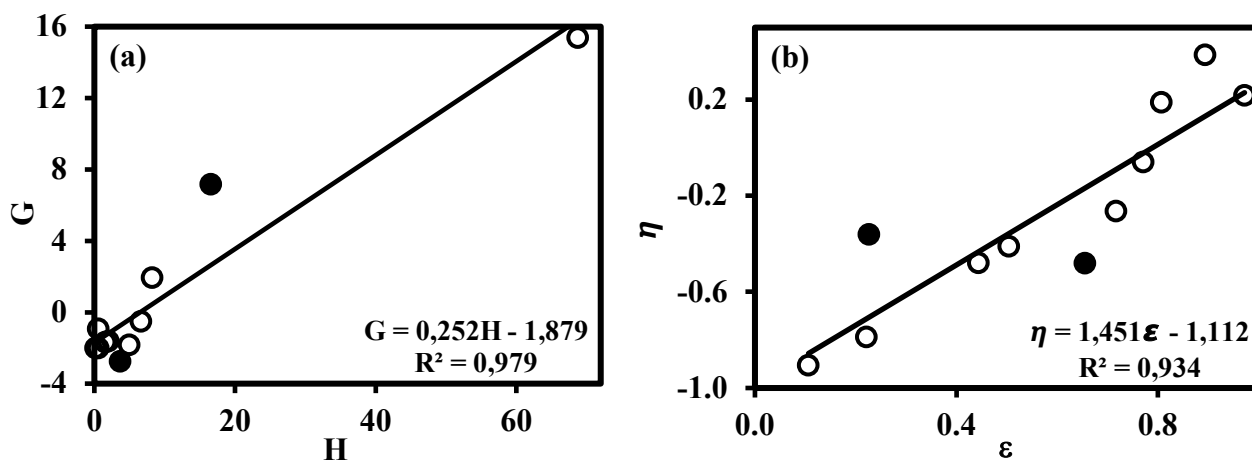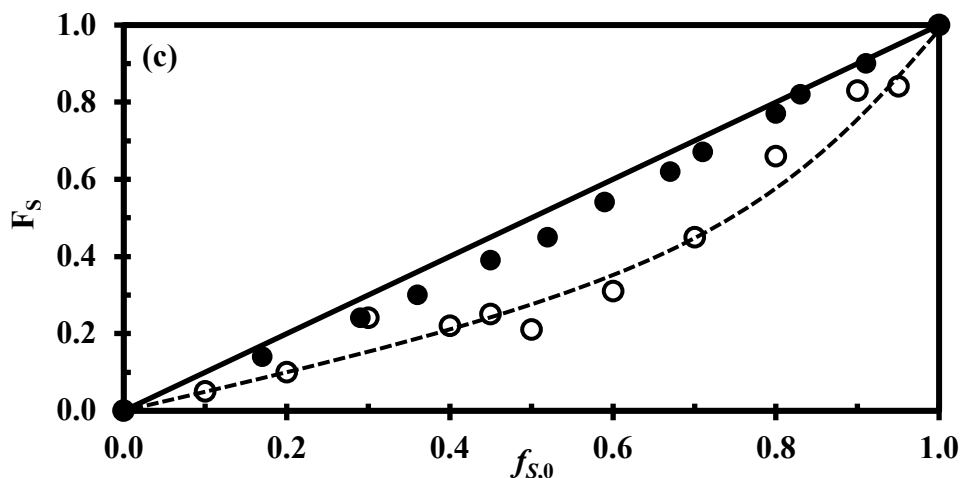
Figure 7. **(a)** FR and **(b)** KT plots to determine the binary reactivity ratios (solid black circles corresponding to experimental outliers not taken into account for the calculations) and **(c)** Mayo-Lewis plot of copolymer composition with respect to S (F_S) *versus* initial styrene feed composition $f_{S,0}$ (experimental data indicated by the open circles (○) while the dotted line is the associated trend line ; solid black circles (•) refer to the data of Trumbo for *My*/S system using conventional radical copolymerization at 65 °C in bulk initiated by azobisisobutyronitrile (AIBN)[14]; The thin straight line indicates the azeotropic composition ($f_{S,0} = F_S$)) for *My* and S statistical copolymerizations done in bulk at 110 °C using NHS-BB. See Supporting Information for the full characterization of the samples used.

� **Effect of feed composition on kinetics.**

The initial molar feed composition of S ($f_{S,0}$) not only influences the copolymer composition but also influences the polymerization kinetics. $<k_p><K>$ kinetic values for this binary system (the product of the average propagation rate constant $<k_p>$ and the average

equilibrium constant <K>) are given in Table 6, which introduces the final molecular characterization of the various copolymers as well (semi-logarithmic plot of overall conversion $ln((1-X_{NMR})^{-1})$ *versus* time, M_n *versus* X_{NMR} plot and Đ *versus* X_{NMR} plot provided in the Supporting Information, Figures S10, S11 and S12 respectively). All of the GPC chromatograms indicated the distributions were monomodal as illustrated in Figure 8 for the experiment *My*/S-50. Furthermore, dispersity *versus* overall conversion plot displayed a Poisson-like distribution (Đ ≈ 1 + 1/DP_n)[102] for every experiment with relatively broad Đ values at the early stages at $X_{NMR} < 0.20$ ($X_{My} < 0.26$ and $X_S < 0.17$) and narrower ones during the subsequent stages of the copolymerization. Such a kinetic feature highlights a rapid initiation with respect to propagation and negligible chain-transfer and termination reactions.

For $f_{S,0} = 0.10$-0.69, the initial molar composition of the mixture did not significantly affect the copolymerization kinetics. The overall polymerization rate was relatively low with $<k_p><K> = 1.11$-2.21 10^{-5} s^{-1} and $X_{NMR} \leq 0.52$ ($X_{My} \leq 0.56$ and $X_S \leq 0.47$) after 7 h. The first-order kinetic behavior was strongly marked as observed with the linear trend of the $ln((1-X_{NMR})^{-1})$ *versus* time curves ($R^2 \geq 0.96$ from 0 to 420 min). This kinetic behavior was closely similar to that of *My* homopolymerization under the same experimental conditions (experiment *My*-5, Table 1 and Table 2). Accordingly, for $f_{S,0} < 0.70$, the copolymerization kinetics was governed by the monoterpene kinetics. Besides, a good control of the reactions was observed with M_n increasing linearly with X_{NMR} and slightly plateauing at higher conversions (M_n on average 87 % of $M_{n,theo}$ at the end of the experiments) and Đ ≤ 1.43 from the onset to the end of these copolymerizations.
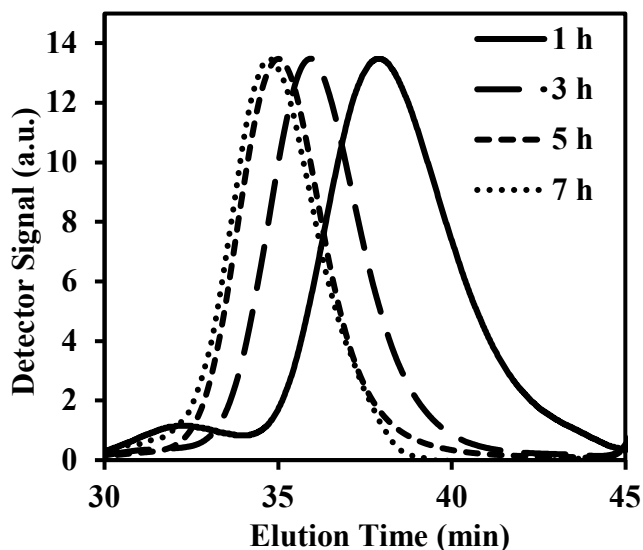
Figure 8. Normalized GPC traces of P(*My-stat*-S) copolymer initiated by NHS-BB at 110 °C in toluene targeting $M_{n,theo} = 30$ kg.mol^{-1} at quantitative conversion (experiment *My*/S-50).

For $f_{S,0} = 0.80$-0.94, *My*/S statistical copolymerizations were faster as indicated in Table 6 by the higher $<k_p><K>$ values (2.03-4.11 10^{-5} s^{-1}) and the almost quantitative overall conversions at the end of the experiments ($X_{NMR} \geq 0.80$ with $X_{My} \geq 0.76$ and $X_S \geq 0.81$). This was likely due to the higher homopropagation rate constant for S ($k_{p,S}$) compared to that of *My*. Homopolymerization of S (experiment *My*/S-100) exhibited $k_pK = 7.46$ 10^{-5} s^{-1} approximately one order of magnitude greater than that for *My* homopolymerization ($k_pK = 1.64$ 10^{-5} s^{-1}), under the same reaction conditions. The propagation rate constants for the radical polymerization of S and I initiated by di-*tert*-butyl peroxide at 5 °C were $k_{p,S} = 180 \pm 10$ L.mol^{-1}.s^{-1} and $k_{p,I} = 125 \pm 30$ L.mol^{-1}.s^{-1} [103]. Similar trend was reported previously for the radical photopolymerization of S

51

at 60 °C with 2-azobispropane as sensitizer ($k_{p,S}$ = 176 L.mol^{-1}.s^{-1})[104] and for the emulsion

polymerization of I at 60 °C with diisopropylbenzene

monohydroperoxide/tetraethylenepentamine (DIBHP/TEPA) catalyst system ($k_{p,I}$ = 50 L.mol^{-1}.s^{-1})[105]. The lower propagation rate constant reported regarding the free radical polymerization of I

compared to that of S is consistent with the kinetic data obtained herein for the NMP of *My* and

S.

The higher overall conversions achieved for $f_{S,0}$ > 0.70 resulted in an apparent loss of

control. Indeed, non-linear *ln*$((1-X_{NMR})^{-1})$ *versus* time curves combined with higher deviations

of experimental average molar masses from the predicted line were observed. M_n were on

average 58 % of $M_{n,theo}$ at the end of the experiments *My*/S-80, *My*/S-90 and *My*/S-95. It should

be first noted that the linear PS standards used for calibrating the GPC might not be very

accurate for these statistical copolymers containing F_{My} = 0.16-0.34. The differences in

hydrodynamic volumes of these copolymers having flexible C6/C8 side chains and that of the PS

standards may be apparent. Although corrections were made using Mark-Houwink-Sakurada

equation, the only MHS coefficients found for P(*My*) may not be perfectly appropriate for this

study. Indeed, $K_{P(My)}$ and $\alpha_{P(My)}$ were obtained at 30 °C for a broad average molar mass range of

1,4-P(*My*)s (M_n = 6.3-55.5 kg.mol^{-1}) with 10 mol% of 3,4-content. However, such significant

deviations cannot be only attributed to the GPC data. It is likely that irreversible termination

reactions became more prevalent at high conversions resulting in a loss the SG1 functionality on

the chain-end and thus more dead chains. Chain transfer side reactions to monomer, generating

monomeric radicals giving rise to a population of very short chains, was well-investigated for the

NMP of styrene[106,107]. Even at a temperature as low as 110 °C, NMP of S in toluene mediated by

SG1 generated a significant population of new short chains presumably due to chain transfer to

S[108]. For this polymerization, it was reported that the total number of chains increased linearly with conversion, resulting in a gradual increase in Đ combined to a plateau of $M_n < M_{n,theo}$. Despite of higher overall polymerization rates, My/S copolymerizations for $f_{S,0} > 0.70$ still exhibited relatively narrow molecular weight distributions (Đ ≤ 1.37).

◘ **Active feature of *My*-rich and S-rich P(*My-stat*-S) copolymers.**

Two different *My*/S statistical copolymers, namely *My*/S-07 ($F_S = 0.07$, *My*-rich P(*My-stat*-S)) and *My*/S-55 ($F_S = 0.55$, S-rich P(*My-stat*-S)), were synthesized under the same previous experimental conditions and their chain end fidelity was studied. Table 7.A gives the molecular characterization of *My*/S-07 and *My*/S-55 copolymers. *My*-rich P(*My-stat*-S) macroinitiator was shown to have an elevated fraction of chain-end nitroxide groups (~ 94 ± 6 mol% SG1 chain-end functionality, standard deviation derived from the difference in M_n value between the GPC result and the corrected M_n using MHS equation) based upon ^{31}P NMR measurements (see Supporting Information, Figure S5 with diethyl phosphite as an internal reference (the presence of the phosphorus atom in the SG1 molecule was used as a tracer[72,109]). It should be noted that the calculation of the fraction of SG1 groups was done by considering similar relaxation times between diethyl phosphite and the polymer. This was mainly due to a slow copolymerization resulting in a low overall conversion and a negligible contribution of side reactions ($M_{n,1}$ was 89 % of $M_{n,theo,X1}$ and Đ < 1.3). S-rich P(*My-stat*-S) macroinitiator contained a lower "living" chain fraction (~ 72 ± 5 mol%), due to a higher overall conversion achieved leading to a slight loss of control ($M_{n,1}$ was 81 % of $M_{n,theo,X1}$).

Table 7. Chain-extensions of **A)** *My*-rich and S-rich P(*My-stat*-S) macroinitiators with **B)** *My* and S monomers in 50 wt% toluene or in bulk and **C)** molecular characterization of the resulting chain-extended products.

A. Macroinitiator[a]							
ID	$f_{S,0}$	$F_{S,1}$	F_{SG1}[b]	X_1	$M_{n,1}$ (kg.mol^{-1})	$M_{n,theo,X1}$[c] (kg.mol^{-1})	$Đ_1$
My/S-07	0.20	0.07	0.94 ± 0.05	0.33	11.7	13.2	1.29
My/S-55	0.79	0.55	0.72 ± 0.04	0.52	16.9	20.8	1.34

B. Formulation of chain-extension							
ID	**[Macroinitiator]$_0$** (M)	**[My]$_0$** (M)	**[S]$_0$** (M)	**[Toluene]$_0$** (M)	$M_{n,theo}$[d] (kg.mol^{-1})	**T (°C)**	t (min)
My/S-07-*My*.a	0.005	2.80	0	4.82	83.7	110	180
My/S-07-*My*.b	0.010	5.79	0	0	89.0	120	300
My/S-07-S	0.005	0	3.67	4.76	84.0	110	180

My/S-55-My.a	0.006	2.53	0	4.81	75.9	110	180
My/S-55-My.b	0.010	5.41	0	0	90.1	120	300
My/S-55-S	0.006	0	3.31	4.98	75.9	110	180

C. Chain-extended copolymer[a]

ID	X_2	$F_{S,2}$	$M_{n,2}$ (kg.mol^{-1})	$M_{n,theo,X2}$[e] (kg.mol^{-1})	$Đ_2$
My/S-07-My.a	0.16	0.06	21.0	23.2	1.35
My/S-07-My.b	0.48	0.02	30.4	48.8	1.59
My/S-07-S	0.38	0.69	34.5	39.2	1.43
My/S-55-My.a	0.15	0.37	22.4	25.8	1.44
My/S-55-My.b	0.57	0.19	40.7	58.6	2.59
My/S-55-S	0.44	0.80	36.4	42.9	1.60

a) The indexes "1" and "2" refer respectively to the final features of the P(*My-stat*-S) macroinitiator and the whole chain-extended P(*My-co*-S) copolymer (macroinitiator + P(*My*) or PS segment added).

b) F_{SG1} corresponds to the living molar fraction of macroinitiator chains terminated by a SG1 unit and was measured by ^{31}P NMR in CDCl$_3$.

c) $M_{n,theo,X1}$ corresponds to the predicted $M_{n,1}$ at the respective X_1 measured experimentally and was calculated as follows: $M_{n,theo,X1} = X_1 \, M_{n,theo,1}$ with $M_{n,theo,1} = 40$ kg.mol^{-1} at $X = 1.0$.

d) $M_{n,theo}$ corresponds to the targeted number-average molecular weight of the whole chain-extended P(*My-stat*-S) copolymer at $X = 1.0$.

e) $M_{n,theo,X2}$ corresponds to the predicted $M_{n,2}$ of the whole chain-extended P(*My-stat*-S) copolymer (macroinitiator + second block added) at the respective X_2 measured experimentally and was calculated as follows: $M_{n,theo,X2} = X_2 \, (M_{n,theo} - M_{n,1}) + M_{n,1}$ (= Predicted M_n of the second block added at conversion X_2 + experimental M_n of the macroinitiator).

In order to confirm the active feature of these two macroinitiators first characterized spectroscopically, two sets of tests were then performed to evaluate the effectiveness of the expected SG1-capped copolymers to cleanly initiate a second batch of monomer: chain-

extensions of *My*/S-07 and *My*/S-55 with *My* (experiments *My*/S-07-*My*.a and *My*/S-55-*My*.a in Table 7.B) and S (experiments *My*/S-07-S and *My*/S-55-S in Table 7.B) monomers at 110 °C in 50 wt% toluene for 3 h. Accordingly, the influence of the composition of P(*My*-*stat*-S) macroinitiators over their ability to polymerize a second batch of monomer was discussed as well as their own versatility to chain-extend *My* and S. The final characterization of the chain-extended products is shown in Table 7.C. *My*-rich macroinitiator *My*/S-07 cleanly chain-extended *My* and S as demonstrated by the low dispersities obtained (Đ ≤ 1.43) and the low deviations of the experimental $M_{n,2}$ values of the chain-extended copolymers from the theoretical ones ($M_{n,2}/M_{n,theo,X2} \geq 88$ %) at the corresponding conversion X_2. Likewise, successful chain-extensions with *My* and S were performed from S-rich macroinitiator *My*/S-55 even though broader molecular weight distributions (Đ = 1.44 with *My* and 1.60 with S) were measured than those of the first set of chain-extensions (Đ = 1.35 and 1.43) and slightly higher deviations of $M_{n,2} \geq 85$ % of $M_{n,theo,X2}$. This minor loss of control can be directly related to the intrinsic features of the S-rich macroinitiator *My*/S-55 having likely a greater proportion of irreversibly terminated chains relative to the My-rich macroinitiator *My*/S-07. Accordingly, the living feature of both *My*-rich and S-rich P(*My*-*stat*-S) macroinitiators was confirmed as also observed by the monomodal nature and the clear shift to the left of the GPC traces corresponding to the chain-extended products (see Supporting Information, Figures S13). Furthermore, both *My* and S monomers were able to be cleanly added to the macroinitiators with slower *My* chain-extension kinetics as previously highlighted in comparison to *My*/S copolymerization kinetics. Indeed, X = 0.15-0.16 were achieved after 3 h reaction for each chain-extension with *My* resulting in the addition of relatively short elastomeric block ≤ 9.3 kg.mol^{-1} (we did not let the polymerization occur for long enough).

Chain-extensions with *My* from *My*/S-07 macroinitiator (experiment *My*/S-07-*My*.b in Table 7.C) and from *My*/S-55 macroinitiator (experiment *My*/S-55-*My*.b in Table 7.C) in bulk at 120 °C for 5 h were then performed in order to increase the polymerization rate. As expected, faster chain-extensions were achieved with X = 0.31 at 3h for experiment *My*/S-07-*My*.b and X = 0.39 at 3h for experiment *My*/S-55-*My*.b compared to lower X = 0.15-0.16 at 3 h in toluene at 110°C. Furthermore, the final conversions X ≥ 0.48 at 5 h (Table 7.C) for the chain-extensions performed in bulk at 120 ºC were significantly greater. Interestingly, the number-average degree of polymerization of the bloc added for the chain-extensions *My*/S-07-*My*.b and *My*/S-55-*My*.b more than doubled with a P(*My*) segment added exhibiting $M_n \geq 18.7$ kg.mol^{-1} compared to previous experiments *My*/S-07-*My*.a and *My*/S-55-*My*.a in toluene at 110 °C. Nonetheless, the higher polymerization rate observed for *My* chain-extensions in bulk at 120 ºC resulted in a marked loss of control as indicated by the broadening of Đ ($Đ_2 \geq 1.59$) and significant deviations of experimental molar masses compared to the predicted ones ($M_{n,2}/M_{n,theo,X2} \geq 62\%$). Non-negligible tails, especially for experiment *My*/S-55-*My*.b, can be observed on the GPC traces (see Supporting Information, Figure S13), likely due to the presence of "dead" chains from the macroinitiators and irreversible terminations.

D) Thermal analysis of the synthesised NMP-based polymers

Thermogravimetric analysis (TGA) was first performed to evaluate the thermal stability of the *My*-based polymers. The decomposition temperatures for P(*My*) and PS homopolymers as

well as P(*My*-*b*-S) diblock copolymers are given in Table 8 (TGA thermograms provided in the Supporting Information, Figure S14). P(*My*) exhibiting M_n = 30.4 kg.mol^{-1} and containing 79 % of 1,4-microstructure (*My*-12) showed a single degradation peak at $T_{dec,max}$ = 385 °C with the sample weight dramatically falling after the onset of decomposition at $T_{dec,1}$ ~ 290 °C, preceded by a first weight loss at T ~ 195 °C. This early significant loss of weight (~ 35 %) can likely be attributed to the presence of unreacted *My* ($T_{b,My}$ = 167 °C) and its impurities such as limonene ($T_{b,My}$ = 176 °C) and volatile isomers and dimers of *My*.. Indeed, TGA analysis for the macroinitiator *My*-12 was performed after drying the sample under air flow without any purification step by dissolution / precipitation cycles. Taking the final NMR conversion of 58 % into account, it can be assumed that an important amount of *My* remained in the P(*My*) matrix. $T_{dec,max}$ = 425-427 °C for persulfate (47 % 1,4-content) and redox (~ 100 % 1,4-content) initiated P(*My*)s, which had respectively M_n = 92.9-109.8 kg.mol^{-1} were previously measured[16]. The slightly better thermal stability achieved compared to the NMP-based sample can be mainly explained by the total absence of nitroxide at the polymer chain-end of persulfate and redox initiated P(*My*)s. NMP-based P(*My*) chains prepared herein are in a majority terminated by a nitroxide group. Since the polymer-nitroxide bond is thermally instable, homolytic cleavage at high temperature can occur, leading to side reactions (backbiting, chain-scission) and resulting in a lower thermal stability[110]. Moreover, the significantly higher M_n exhibited by persulfate and redox initiated P(*My*)s could have contributed to the higher $T_{dec,max}$ as well. NHS-BB initiated PS (*My*/S-100) exhibited a two-step degradation pattern with the sample weight gradually falling from 190 °C, likely due to the evaporation of residual styrene and volatile oligomers, until it reached about 370 °C, where beyond that the polymer degraded rapidly. PS $T_{dec,max}$ was 445 °C, which is consistent with poly(styrene)s of similar molecular weights[111]. Both *My*-11-Sa and *My*-

10-S P(*My-b*-S) diblock copolymers showed the same two-step degradation pattern with a slight weight loss from T ~ 150 °C to T ~ 350 °C followed by the main degradation peak. P(*My-b*-S) diblock copolymers, with $T_{dec,max}$ = 435-440 °C, exhibited a thermal stability similar to that of PS homopolymer.

Table 8. Glass transition temperatures (T_gs) and decomposition temperatures (T_{dec}s) for P(*My*) (*My*-12), PS (*My*/S-100) and P(*My-b*-S) diblock copolymers (*My*-10-S, *My*-11-Sa, *My*-11-Sb and *My*-12-S).

ID	F_S	$T_g^{(a)}$ (°C)	$T_{dec,1}^{(b)}$ (°C) [b]	$T_{dec,max}$ (°C)	$T_{dec,2}^{(b)}$ (°C)
My-12	0	− 77	290	385	485
My-12-S	0.27	− 63	-	-	-
My-11-Sb	0.39	− 77	-	-	-

My-11-Sa	0.47	− 73 / + 61[i]	140	440	490
My-10-S	0.62	− 70 / + 57	155	435	490
My/S-100	1.0	+ 77	190	445	490

---

[i] DSC thermogram in Figure 9.

a) T_g('s) measured by DSC under nitrogen atmosphere at a rate of 10 °C.min^{-1} using three scans per cycle (heat/cool/heat).

b) $T_{dec,1}$ (onset of decomposition), $T_{dec,max}$ (temperature at which weight loss is most apparent) and $T_{dec,2}$ (end of decomposition) measure by thermogravimetric analysis (TGA) under nitrogen flow at a ramp rate of 10 °C.min^{-1} (TGA thermograms provided in the Supporting Information).

Differential scanning calorimetry (DSC) measurements were then performed to determine glass transition temperatures (T_gs) for P(*My*), PS and P(*My-b*-S) diblock copolymers. Table 8 shows measured T_gs (DSC plots with changes in the slope provided in the Supporting Information, Figures S15 and S16). As expected, P(*My*), as an amorphous elastomer, had a $T_g = -77$ °C much below the ambient temperature and very close to the natural rubber *cis*-1,4-PI, which has T_g around -73 °C[112]. NMP-based PS exhibiting $M_n = 15.6$ kg.mol^{-1} had a $T_g = +77$ °C instead of 100-110 °C for atactic PS with $M_n > 100$ kg.mol^{-1} [113]. Beyond the critical influence of M_n on T_g, the possible presence of oligomers in the PS matrix, behaving as plasticizers, could play a minor role in lowering the glass transition temperature. S-rich diblock copolymers,

namely *My*-10-S and *My*-11-Sa, showed two separated T_gs: a first one at about $-70\ °C$

corresponding to the soft P(*My*) block and a second one around $+60\ °C$ corresponding to the

hard PS block. This is illustrated in Figure 9 by the changes in slope of the DSC trace for *My*-11-

Sa sample.

Figure 9. DSC trace (second heating run) of P(*My-b*-S) diblock copolymer *My*-11-Sa. The grey arrows indicate the changes in slope observed. DSC traces of the other P(*My-b*-S) diblock copolymers can be found in the Supporting Information.
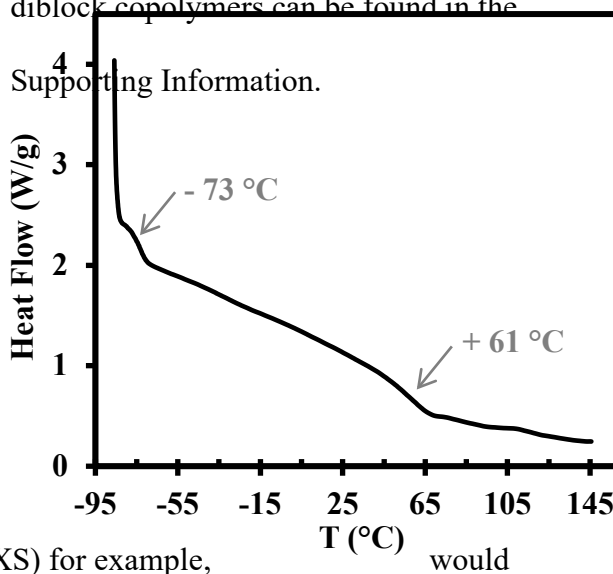
This suggests the possible micro-phase separation of these two heterogeneous phases. However, an in-depth analysis of the P(*My-b*-S)s phase behavior, including atomic force microscopy (AFM) and small-angle X-ray scattering (SAXS) for example, would

demontrate whether or not a micro-phase separation is apparent and determine the morphology

of this latter. It can be noted that the T_gs of these diblocks did not exactly correspond to the T_gs

of the respective P(*My*) and PS homopolymers. This might be due to a partial miscibility of the

two blocks caused by both a relatively low M_n and a vulnerable phase separation taking the

structural similarities between *My* and S repetitive units into account. Partial mixing of PI and PS

blocks were previously observed for P(I-*b*-S) diblocks leading to in-between glass transition

63

temperatures[114]. Interestingly, for *My*-rich diblock copolymers (*My*-11-Sb and *My*-12-S) with F_S ≤ 0.39, no second glass transition was observed. The T_g for the PS segment was not visible on the DSC thermograms presumably due to a too low PS content. Similarly, as regards *β*-myrcene/*α*-methyl-*p*-methylstyrene *My*/AMMS triblocks with F_{AMMS} < 0.35, even though the T_g for P(*My*) was detectable, no DSC signal corresponding to the T_g of the P(AMMS) outer segments was observed[21]. By contrast, both T_gs for P(I-*b*-S) diblock copolymers were visible even for a large fraction of PS (F_S = 0.78) and the T_g for PI was not observed only for F_S = 0.92[114].

T_g values were also measured for P(*My*-*stat*-S) statistical copolymers exhibiting F_S = 0.08-0.96, as presented in Figure 10 (DSC traces given in the Supporting Information, Figure S16). Evidently, as the final molar content of styrene in the copolymer increased, T_g increased due to the pendant aromatic groups of S repeat units, providing rigidity and hardness. An exponential trend was observed with liquid rubber P(*My*-*stat*-S) copolymers achieved for F_S ≤ 0.48, exhibiting T_g < − 40 °C. A more significant dependence of T_g on F_S was apparent for S-rich copolymers. Indeed, T_gs ranged from − 9 °C to + 77 °C for F_S = 0.66-1.00. This may be explained by the sequence distribution of *My* repetitive units within the polymer chains. The propagating species has a clear preference for *My*, even at a low molar fraction of *My* in the final copolymer, and short P(*My*) segments can be formed, resulting in "elastomeric knots" in the matrix. These peculiar connections, exhibiting a high flexibility with long side chains, may significantly disrupt the PS network. Theoretical T_g, $T_{g,th}$, for these copolymers can be predicted by the Fox equation[115] (7) where w_{My} and w_S are the weight fractions of *My* and S, and $T_{g,My}$ and $T_{g,S}$ are the experimental T_gs of P(*My*) and PS homopolymers.

$$1/T_{g,th} = w_{My}/T_{g,My} + w_S/T_{g,S} \quad (7)$$

Figure 10 also includes the Fox equation predictions of the P(My-$stat$-S) T_gs. Non-negligible deviations can be noticed from our experimental data and explained by the limitations of the Fox equation in its prediction of the glass transition temperatures. Basically, it is a simple bulk additive relation disregarding the sequence distribution of My and S monomer units in the copolymer[116]. My, containing two isoprene units, is a monoterpene structurally related to the readily available petro-chemical isoprene (I)[3]. Both P(My) and poly(isoprene) PI polymers are elastomers, exhibiting a maximum glass transition temperature $T_{g,\infty}$ between $-$ 70 °C and $-$ 80 °C[117]. It is thereby worthwhile to compare the T_gs of P(My-$stat$-S)s with those of P(I-$stat$-S) copolymers. Interestingly, a similar dependence of T_g on F_S was reported by Halasa and coworkers for P(I-ran-S) random copolymers[118] as shown in Figure 10. The higher T_gs measured can be mainly attributed to the higher experimental T_g for PI ($-$ 65 °C) than that of P(My) ($-$ 77 °C) and the greater M_n > 120 kg.mol^{-1} exhibited by the various P(I-ran-S) copolymers.
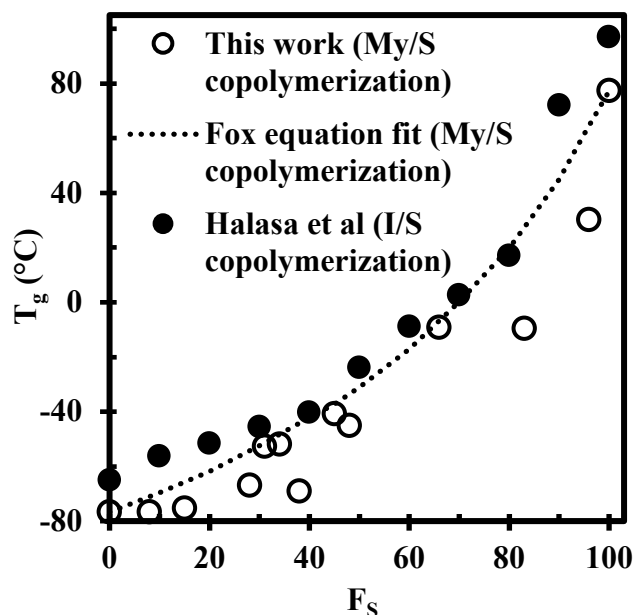
Figure 10. F_S effects on T_g in P(*My-stat*-S) statistical copolymers (open circles). All of the DSC traces are given in the Supporting Information. The Fox equation predictions of the P(*My-stat*-S) T_gs are represented by the dotted line. The black solid circles refer to Halasa et al's data for P(I-*ran*-S) random copolymers produced by anionic polymerization at 65 °C using a catalyst system of various sodium dodecylbenzene sulfonate (SDBS) to *n*-butyllithium (*n*-BuLi) ratios[118].

CONCLUSION.

In this study, the optimized NMP of *My* was accomplished at 120 °C in bulk initiated by the alkoxyamine NHS-BB without requiring additional SG1 free nitroxide. Relatively low apparent rate constant ($k_p K_{My} = 4.3\ 10^{-5}\ s^{-1}$) compared to S homopolymerization by NMP, first-order kinetic behavior (linear trend of $ln((1-X_{My})^{-1})$ *versus* time with $R^2 > 0.99$) and M_n increasing linearly with X_{My} (M_n on average 90 % of $M_{n,theo}$) were apparent under these

experimental conditions when targeting moderate $M_{n,theo} \sim 30$ kg.mol^{-1} at complete conversion. Resulting *cis*-1,4-rich P(*My*) containing 1,2- and 3,4-defects (< 20 %) and exhibiting Đ < 1.30 was achieved. Its T_g and decomposition temperature $T_{dec,max}$ were − 77 °C and + 385 °C, respectively. The active feature of the NMP-based P(*My*) macroinitiator was confirmed by subsequent chain-extensions with S leading to well-defined P(*My-b*-S) diblock copolymers, retaining their monomodal nature. S-rich P(*My-b*-S)s showed two separate T_gs, at about − 70 °C and + 60 °C, indicating possibly their micro-phase separation. P(*My-b*-S) diblocks exhibited better thermal stability ($T_{dec,max}$ = 435-440 °C) than P(*My*) and poor strain-stress properties with ultimate tensile strength < 0.9 MPa and tensile elongation at break < 14 %. This brittle behavior combined with a low extensibility can be largely explained by a lack of entanglement density due to the experimental P(*My*) M_n = 13.2-30.4 kg.mol^{-1}, lower than or equal the P(*My*) entanglement molecular weight ($M_{e,P(My)}$ = 22-31 kg.mol^{-1})[81]. Statistical copolymers from *My* and S were also prepared by NMP with $f_{S,0}$ = 0.10-0.94 at 110 °C in bulk using NHS-BB. The Fineman-Ross approach yielded r_{My} = 1.88 ± 0.12 and r_S = 0.25 ± 0.04 ($r_{My} \times r_S$ = 0.47 ± 0.11) whereas r_{My} = 2.19 ± 0.07 and r_S = 0.34 ± 0.19 ($r_{My} \times r_S$ = 0.74 ± 0.41) were determined by Kelen-Tüdös approach. Well-controlled copolymerizations were performed with resulting P(*My-stat*-S)s exhibiting M_n = 8.2-19.8 kg.mol^{-1}, Đ < 1.40 and monomodal distributions as shown by the GPC chromatograms. P(*My-stat*-S)s displayed a glass transition temperature between − 77 and + 30 °C depending on the molar composition of S in the statistical copolymer. The high chain-end fidelity of *My*-rich and S-rich P(*My-stat*-S)s was confirmed via successful chain-extensions with both *My* and S. This investigation thereby presented a robust and simple way to synthesize P(*My*), P(*My-b*-S) and P(*My-stat*-S) by NMP.

ASSOCIATED CONTENT

Supporting Information

The Supporting Information is available free of charge on the ACS Publications website.

Spectra of isolated *My*-based polymer samples (^{1}H, ^{13}C and ^{31}P NMR), additional GPC traces, DSC traces and stress-strain curves, TGA thermograms, theoretical background (FR, KT and NLLS approaches) and experimental details for *My*/S statistical copolymerization

AUTHOR INFORMATION

Corresponding Author

*E-mail: milan.maric@mcgill.ca (M.M.)

REFERENCES

(1) Sylvestre, A. J. D.; Gandini, A. Rosin: Major Sources, Properties and Applications. In *Monomers, Polymers and Composites from Renewable Resources*, 1ˢᵗ ed.; Belgacem, M. N., Gandini, A., Eds.; Elsevier: Oxford, **2008**; 67-88.

(2) Wilbon, P. A.; Chu, F.; Tang, C. Progress in Renewable Polymers from Natural Terpenes, Terpenoids, and Rosin. *Macromol. Rapid Commun*. **2013**, *34* (1), 8-37.

(3) Behr, A.; Johnen, L. Myrcene as a Natural Base Chemical in Sustainable Chemistry: A Critical Review. *ChemSusChem* **2009**, *2* (12), 1072-1095.

(4) Goldblatt, L. A.; Palkin, S. Process for Converting Nopinene to Myrcene. U.S. Patent US2420131A, **1947**.

(5) Savich, T. R.; Goldblatt, L. A. Process for Producing Myrcene from Beta-Pinene. U.S. Patent US2507546, **1950**.

(6) Wattimena, F. Isomerization of Terpene Compounds. U.S. Patent US4108917A, **1978**.

(7) Yermakova, A.; Chibiryaev, A. M.; Kozhevnikov, I. V.; Anikeev, V. I. The Kinetics of Thermal Isomerization of β-Pinene and a Mixture of β- and α-Pinenes in Supercritical Ethanol. *J. Supercrit. Fluids* **2008**, *45* (1), 74-79.

(8) Kolicheski, M. B.; Cocco, L. C.; Mitchell, D. A.; Kaminski, M. Synthesis of Myrcene by Pyrolysis of β-Pinene: Analysis of Decomposition Reactions. *J. Anal. Appl. Pyrolysis* **2007**, *80* (1), 92-100.

(9) Marti, A. New Styrenic Materials, a Natural Alternative to B in ABS. Chalmers University of Technology **2014**.

(10) Cawse, J. L.; Stanford, J. L.; Still, R. H. Polymers from Renewable Sources: 5. Myrcene Based Polyols as Rubber-Toughening Agents in Glassy Polyurethanes. *Polymer* **1987**, *28* (3), 368-374.

(11) Johanson, A. J.; McKennon, F. L.; Goldblatt, L. A. Emulsion Polymerization of Myrcene. *Ind. Eng. Chem.* **1948**, *40* (3), 500-502.

(12) Cawse, J. L.; Stanford, J. L.; Still, R. H. Polymers from Renewable Sources: 4. Polyurethane Elastomers based on Myrcene Polyols. *J. Appl. Polym. Sci.* **1986**, *31* (6), 1549-1565.

(13) Cawse, J. L.; Stanford, J. L.; Still, R.H. Polymers from Renewable Sources: 3. Hydroxy-Terminated Myrcene Polymers. *J. Appl. Polym. Sci.* **1986**, *31* (7), 1963-1975.

(14) Trumbo, D. L. Free Radical Copolymerization Behavior of Myrcene: I. Copolymers with Styrene, Methyl Methacrylate or *p*-Fluorostyrene. *Polym. Bull.* **1993**, *31*, 629-636.

(15) Choi, S. W.; Ritter, H. Novel Polymerization of Myrcene in Aqueous Media via Cyclodextrin-Complexes. *e-Polymers* **2007**.
DOI: 10.1515/epoly.2007.7.1.527

(16) Sarkar, P.; Bhowmick, A. K. Synthesis, Characterization and Properties of a Bio-based Elastomer: Polymyrcene. *RSC Adv.* **2014**, *4*, 61343-61354.

(17) Loughmari, S.; Hafid, A.; Bouazza, A.; El Bouadili, A.; Zinck, P.; Visseaux, M. Highly Stereoselective Coordination Polymerization of *β*-Myrcene from a Lanthanide-based Catalyst:

Access to Bio-Sourced Elastomers. *J. Polym. Sci., Part A: Polym. Chem.* **2012**, *50* (14), 2898-2905.

(18) Sivola, A. *N*-Butyllithium-Initiated Polymerization of Myrcene and its Copolymerization with Styrene. *Acta Polytech. Scand.-Chem. Technol. Ser.* **1977**, *134*, 7-65.

(19) Quirk, R. P.; Huang, T.-L. Alkyllithium-Initiated Polymerization of Myrcene: New Block Copolymers of Styrene and Myrcene. In *New Monomers and Polymers*; Culbertson, B. M., Pittman Jr, C. U., Eds.; Springer-Plenum Press: New York, **1984**; 329-355.

(20) Quirk, R. P. Research on Anionic Triblock Copolymers. In *Thermoplastic Elastomers,* 3rd ed.; Calhoun, A., Holden, G., Kricheldorf, H. R., Eds.; Hanser Gardner Publications: Cincinnati, **2004**; 69-91.

(21) Bolton, J. M.; Hillmyer, M. A.; Hoye, T. R. Sustainable Thermoplastic Elastomers from Terpene-Derived Monomers. *ACS Macro Lett.* **2014**, *3*, 717-720.

(22) Nicolas, J.; Guillaneuf, Y.; Lefay, C.; Bertin, D.; Gigmes, D.; Charleux, B. Nitroxide-Mediated Polymerization. *Prog. Polym. Sci.* **2013**, *38* (1), 63-235.

(23) Chiefari, J.; Chong, Y.; Ercole, F.; Krstina, J.; Jeffery, J.; Le, T.; Mayadunne, R.; Meijs, G.; Moad, C.; Moad, G.; Rizzardo, E.; Thang, S. Living Free-Radical Polymerization by Reversible Addition-Fragmentation Chain Transfer: The RAFT Process. *Macromolecules* **1998**, *31*, 5559-5562.

(24) Braunecker, W. A.; Matyjaszewski, K. Controlled/Living Radical Polymerization: Features, Developments, and Perspectives. *Prog. Polym. Sci.* **2007**, *32* (1), 93-146.

(25) Georges, M. K.; Veregin, R. P. N.; Kazmaier, P. M.; Hamer, G. K. Narrow Molecular Weight Resins by a Free-Radical Polymerization Process. *Macromolecules* **1993**, *26* (11), 2987-2988.

(26) Veregin, R. P. N.; Georges, M. K.; Kazmaier, P. M.; Hamer, G. K. Free Radical Polymerizations for Narrow Polydispersity Resins: Electron Spin Resonance Studies of the Kinetics and Mechanism. *Macromolecules* **1993**, *26* (20), 5316-5320.

(27) Wang, J.-S.; Matyjaszewski, K. Controlled/"Living" Radical Polymerization. Atom Transfer Radical Polymerization in the Presence of Transition-Metal Complexes. *J. Am. Chem. Soc.* **1995**, *117* (20), 5614-5615.

(28) Hadjichristidis, N.; Pispas, S.; Floudas, G. *Block Copolymers: Synthetic Strategies, Physical Properties, and Applications*; John Wiley & Sons: New Jersey, **2003**; 3-65.

(29) Solomon, D. H.; Rizzardo, E.; Cacioli, P. New Polymerization Process and Polymers Produced Thereby. Eur. Pat. Appl. 0135280A3, **1985**.

(30) di Lena, F.; Matyjaszewski, K. Transition Metal Catalysts for Controlled Radical Polymerization. *Prog. Polym. Sci.* **2010**, *35* (8), 959-1021.

(31) Matyjaszewski, K. Controlled Radical Polymerization: State of the Art in 2008. In *Controlled/Living Radical Polymerization: Progress in ATRP*; Matyjaszewski, K., Ed.; American Chemical Society: Washington DC, **2009**; 3-13.

(32) Matyjaszewski, K.; Xia, J. Atom Transfer Radical Polymerization. *Chem. Rev.* **2001**, *101* (9), 2921-2990.

(33) Jitchum, V.; Perrier, S. Living Radical Polymerization of Isoprene via the RAFT Process. *Macromolecules* **2007**, *40* (5), 1408-1412.

(34) Moad, G.; Barner-Kowollik, C. The Mechanism and Kinetics of RAFT Process: Overview, Rates, Stabilities, Side Reactions, Product Spectrum and Outstanding Challenges. In *Handbook of RAFT Polymerization*; Barner-Kowollik, C., Ed.; Wiley-VCH: Weinheim, **2008**; 51-104.

(35) Moad, G.; Rizzardo, E.; Thang, S. H. Living Radical Polymerization by the RAFT Process-A Second Update. *Aust. J. Chem.* **2009**, *62* (11), 1402-1472.

(36) Hilschmann, J.; Kali, G. Bio-based Polymyrcene with Highly Ordered Structure via Solvent Free Controlled Radical Polymerization. *Eur. Polym. J.* **2015**, *73*, 363-373.

(37) Hawker, C. J.; Bosman, A. W.; Harth, E. New Polymer Synthesis by Nitroxide Mediated Living Radical Polymerizations. *Chem. Rev.* **2001**, *101* (12), 3661-3688.

(38) Grubbs, R. B. Nitroxide-Mediated Radical Polymerization: Limitations and Versatility. *Polym. Rev.* **2011**, *51*, 104-137.

(39) Keoshkerian, B.; Georges, M.; Quinlan, M.; Veregin, R.; Goodbrand, B. Polyacrylates and Polydienes to High Conversion by a Stable Free Radical Polymerization Process: Use of Reducing Agents. *Macromolecules* **1998**, *31*, 7559-7561.

(40) Georges, M. K.; Hamer, G. K.; Listigovers, N. A. Block Copolymer Synthesis by a Nitroxide-Mediated Living Free Radical Polymerization Process. *Macromolecules* **1998**, *31*, 9087-9089.

(41) Benoit, D.; Harth, E.; Fox, P.; Waymouth, R. M.; Hawker, C. J. Accurate Structural Control and Block Formation in the Living Polymerization of 1,3-Dienes by Nitroxide-Mediated Procedures. *Macromolecules* **2000**, *33* (2), 363-370.

(42) Grubbs, R. B.; Wegrzyn, J. K.; Xia, Q. One-Step Synthesis of Alkoxyamines for Nitroxide-Mediated Radical Polymerization. *Chem. Commun*. **2005**, 80-82.

(43) Wegrzyn, J. K.; Stephan, T.; Lau, R. N.; Grubbs, R. B. Preparation of Poly(ethylene oxide)-*block*-Poly(isoprene) by Nitroxide-Mediated Free Radical Polymerization from PEO Macroinitiators. *J. Polym. Sci., Part A: Polym. Chem.* **2005**, *43* (14), 2977-2984.

(44) Bertin, D.; Gigmes, D.; Marque, S. R. A.; Tordo, P. Kinetic Subtleties of Nitroxide Mediated Polymerization. *Chem. Soc. Rev.* **2011**, *40,* 2189-2198.

(45) Bertin, D.; Gigmes, D.; Marque, S. R. A.; Tordo, P. Polar, Steric, and Stabilization Effects in Alkoxyamines C-ON Bond Homolysis: A Multiparameter Analysis. *Macromolecules* **2005**, *38* (7), 2638-2650.

(46) Benoit, D.; Chaplinski, V.; Braslau, R.; Hawker, C. J. Development of a Universal Alkoxyamine for "Living" Free Radical Polymerizations. *J. Am. Chem. Soc.* **1999**, *121* (16), 3904-3920.

(47) Grimaldi, S.; Finet, J.-P.; Le Moigne, F.; Zeghdaoui, A.; Tordo, P.; Benoit, D.; Fontanille, M.; Gnanou, Y. Acyclic *beta*-Phosphonylated Nitroxides: A New Series of Counter-Radicals for "Living"/Controlled Free Radical Polymerization. *Macromolecules* **2000**, *33*, 1141-1147.

(48) Luo, K.; Rzayev, J. Living Radical Polymerization of Bicyclic Dienes: Synthesis of Thermally Cross-Linkable Block Copolymers. *Macromolecules* **2009**, *42* (23), 9268-9274.

(49) Lessard, B.; Tervo, C.; Marić, M. High-Molecular-Weight Poly(*tert*-butyl acrylate) by Nitroxide-Mediated Polymerization: Effect of Chain Transfer to Solvent. *Macromol. React. Eng.* **2009**, *3*, 245-256.

(50) Lessard, B.; Marić, M. Nitroxide-Mediated Polymerization of Poly(ethylene glycol) Acrylate Comb-Like Polymers. *Macromolecules* **2008**, *41*, 7870-7880.

(51) Lessard, B.; Schmidt, S. C.; Marić, M. Styrene/Acrylic Acid Random Copolymers Synthesized by Nitroxide-Mediated Polymerization: Effect of Free Nitroxide on Kinetics and Copolymer Composition. *Macromolecules* **2008**, *41*, 3446-3454.

(52) Lessard, B.; Graffe, A.; Marić, M. Styrene/*tert*-Butyl Acrylate Random Copolymers Synthesized by Nitroxide-Mediated Polymerization: Effect of Free Nitroxide on Kinetics and Copolymer Composition. *Macromolecules* **2007**, *40*, 9284-9292.

(53) Harrisson, S.; Couvreur, P.; Nicolas, J. SG1 Nitroxide-Mediated Polymerization of Isoprene: Alkoxyamine Structure/Control Relationship and α,ω-Chain-End Functionalization. *Macromolecules* **2011**, *44* (23), 9230-9238.

(54) Vinas, J.; Chagneux, N.; Gigmes, D.; Trimaille, T.; Favier, A.; Bertin, D. SG1-based Alkoxyamine bearing a N-Succinimidyl Ester: A Versatile Tool for Advanced Polymer Synthesis. *Polymer* **2008**, *49* (17), 3639-3647.

(55) Moayeri, A.; Lessard, B.; Marić, M. Nitroxide Mediated Controlled Synthesis of Glycidyl Methacrylate-Rich Copolymers enabled by SG1-based Alkoxyamines bearing Succinimidyl Ester Groups. *Polym. Chem.* **2011**, *2*, 2084-2092.

(56) Zhang, C.; Marić, M. Synthesis of Stimuli-Responsive, Water-Soluble Poly[2-(dimethylamino)ethyl methacrylate/styrene] Statistical Copolymers by Nitroxide Mediated Polymerization. *Polymers* **2011**, *3* (3), 1398-1422.

(57) Marić, M.; Consolante, V. Versatility of a Succinimidyl-Ester Functional Alkoxyamine for Controlling Acrylonitrile Copolymerizations. *J. Appl. Polym. Sci.* **2013**, *127*, 3645-3656.

(58) Georges, S.; Bria, M.; Zinck, P.; Visseaux, M. Polymyrcene Microstructure revisited from Precise High-Field Nuclear Magnetic Resonance Analysis. *Polymer* **2014**, *55*, 3869-3878.

(59) Xie, J. Viscometric Constants for Small Polystyrenes and Polyisobutenes by Gel Permeation Chromatography. *Polymer* **1994**, *35* (11), 2385-2389.

(60) Hattam, P.; Gauntlett, S.; Mays, J. W.; Hadjichristidis, N.; Young, R. N.; Fetters, L. J. Conformational Characteristics of some Model Polydienes and Polyolefins. *Macromolecules* **1991**, *24* (23), 6199-6209.

(61) Pasch, H; Trathnigg, B. *Multidimensional HPLC of Polymers*; Springer: Heidelberg, **2013**; 37-90.

(62) Marque, S. R. A.; Le Mercier, C.; Tordo, P.; Fischer, H. Factors Influencing the C−O−Bond Homolysis of Trialkylhydroxylamines. *Macromolecules* **2000**, *33* (12), 4403-4410.

(63) Charleux, B.; Nicolas, J.; Guerret, O. Theoretical Expression of the Average Activation-Deactivation Equilibrium Constant in Controlled/Living Free-Radical Copolymerization Operating via Reversible Termination. Application to a Strongly Improved Control in Nitroxide-Mediated Polymerization of Methyl Methacrylate. *Macromolecules* **2005**, *38* (13), 5485-5492.

(64) Couvreur, L.; Lefay, C.; Belleney, J.; Charleux, B.; Guerret, O.; Magnet, S. First Nitroxide-Mediated Controlled Free-Radical Polymerization of Acrylic Acid. *Macromolecules* **2003**, *36* (22), 8260-8267.

(65) Charleux, B.; Nicolas, J. Water-Soluble SG1-based Alkoxyamines: A Breakthrough in Controlled/Living Free-Radical Polymerization in Aqueous Dispersed Media. *Polymer* **2007**, *48* (20), 5813-5833.

(66) Roberts, G.; Davis, T.; Heuts, J.; Ball, G. Monomer Substituent Effects in Catalytic Chain Transfer Polymerization: *tert*-Butyl Methacrylate and Dimethyl Itaconate. *Macromolecules* **2002**, *35* (27), 9954-9963.

(67) Beuermann, S.; Buback, M. Rate Coefficients of Free-Radical Polymerization deduced from Pulsed Laser Experiments. *Prog. Polym. Sci.* **2002**, *27* (2), 191-254.

(68) Tebben, L.; Studer, A. Nitroxides: Applications in Synthesis and in Polymer Chemistry. *Angew. Chem. Int. Ed.* **2011**, *50* (22), 5034-5068.

(69) Gryn'ova, G.; Lin, C. Y.; Coote, M. L. Which Side-Reactions Compromise Nitroxide Mediated Polymerization?. *Polym. Chem.* **2013**, *4* (13), 3744-3754.

(70) Moad, G.; Rizzardo, E. Alkoxyamine-Initiated Living Radical Polymerization: Factors Affecting Alkoxyamine Homolysis Rates. *Macromolecules* **1995**, *28* (26), 8722-8728.

(71) Beckwith, A. L. J.; Bowry, V. W.; Ingold, K. U. Kinetics of Nitroxide Radical Trapping. 1. Solvent Effects. *J. Am. Chem. Soc.* **1992**, *114* (13), 4983-4992.

(72) Lefay, C.; Belleney, J.; Charleux, B.; Guerret, O.; Magnet, S. End-Group Characterization of Poly(acrylic acid) Prepared by Nitroxide-Mediated Controlled Free-Radical Polymerization. *Macromol. Rapid Commun.* **2004**, *25* (13), 1215-1220.

(73) Harrisson, S.; Couvreur, P.; Nicolas, J. Use of Solvent Effects to Improve Control over Nitroxide-Mediated Polymerization of Isoprene. *Macromol. Rapid. Commun.* **2012**, *33* (9), 805-810.

(74) Fierens, S. K.; D'Hooge, D. R.; Van Steenberge, P. H. M.; Reyniers, M-. F.; Marin, G. B. MAMA-SG1 Initiated Nitroxide Mediated Polymerization of Styrene: From Arrhenius Parameters to Model-based Design. *Chem. Eng. J.* **2015**, *278*, 407-420.

(75) Runckel, W. J.; Goldblatt, L. A. Inhibition of Myrcene Polymerization during Storage. *Ind. Eng. Chem.* **1946**, *38* (7), 749-751.

(76) Becer, C. R.; Paulus, R. M.; Hoogenboom, R.; Schubert, U. S. Optimization of the Nitroxide-Mediated Radical Polymerization Conditions for Styrene and *tert*-Butyl Acrylate in an Automated Parallel Synthesizer. *J. Polym. Sci., Part A: Polym. Chem.* **2006**, *44* (21), 6202-6213.

(77) McHale, R.; Aldabbagh, F.; Zetterlund, P. B. The Role of Excess Nitroxide in the SG1 (*N*-*tert*-butyl-*N*-[1-diethylphosphono-(2,2-dimethylpropyl)] Nitroxide)-Mediated Polymerization of Methyl Methacrylate. *J. Polym. Sci., Part A: Polym. Chem.* **2007**, *45* (11), 2194-2203.

(78) Hawker, C. J.; Barclay, G. G.; Dao, J. Radical Crossover in Nitroxide Mediated "Living" Free Radical Polymerizations. *J. Am. Chem. Soc.* **1996**, *118*, 11467-11471.

(79) Noshay, A.; McGrath, J. E. A-B-A Triblock Copolymers. *Block Copolymers: Overview and Critical Survey;* Academic Press: New York, **1977**; 186-304.

(80) Morton, M.; McGrath, J. E.; Juliano, P. C. Structure-Property Relationships for Styrene-Diene Thermoplastic Elastomers. *J. Polymer Sci.: Part C* **1969**, *26* (1), 99-115.

(81) Fetters, L. J.; Lohse, D. J; Colby, R. H. Part V. Mechanical Properties: Chain Dimensions and Entanglement Spacings. In *Physical Properties of Polymers Handbook*, 2nd Ed.; Mark, J. E., Ed.; Springer: New York, **2007**; 447-454.

(82) Landel, R. F.; Nielsen, L. E. Stress-Strain Behavior and Strength. *Mechanical Properties of Polymers and Composites*, 2nd Ed.; Marcel Dekker: New York, **1994**; 233-336.

(83) Adhikari, R. Influence of Uncoupled Diblock Molecules on Mechanical Properties of Styrene/Butadiene/Styrene Triblock Copolymers. *Nepal Journal of Science and Technology* **2011**, *12*, 49-56.

(84) Tilley, R. J. D. Physical Properties. *Understanding Solids: The Science of Materials*, 2nd Ed.; John Wiley & Sons: Chichester, **2013**; 289-294.

(85) Jones, D. R. H.; Ashby, M. F. Mechanical Behaviour of Polymers. *Engineering Materials 2: An Introduction to Microstructure, Processing and Design*, 2nd Ed.; Butterworth-Heinemann: Oxford, **1998**; 238-253.

(86) Robinson, R. A.; White, E. F. T. Mechanical Properties of Styrene-Isoprene Block Copolymers. In *Block Polymers*; Aggarwal, S. L., Ed.; Plenum Press: New York, **1970**; 123-136.

(87) Fukuda, T.; Terauchi, T.; Goto, A.; Ohno, K.; Tsujii, Y.; Miyamoto, T.; Kobatake, S.; Yamada, B. Mechanisms and Kinetics of Nitroxide-Controlled Free Radical Polymerization. *Macromolecules* **1996**, *29*, 6393-6398.

(88) Odian, G. Chain Copolymerization. *Principles of Polymerization*, 4th Ed.; John Wiley & Sons: New Jersey, **2004**; 466-505.

(89) Mayo, F. R.; Lewis, F. M. Copolymerization. I. A Basis for Comparing the Behavior of Monomers in Copolymerization; The Copolymerization of Styrene and Methyl Methacrylate. *J. Am. Chem. Soc.* **1944**, *66* (9), 1594-1601.

(90) Fineman, M.; Ross, S. D. Linear Method for Determining Monomer Reactivity Ratios in Copolymerizations. *J. Polym. Sci., Part A: Polym. Chem.* **1950**, *5* (2), 259-262.

(91) Kelen, T.; Tüdös, F. Analysis of the Linear Methods for Determining Copolymerization Reactivity Ratios. I. A New Improved Linear Graphic Method. *J. Macromol. Sci. Chem.* **1975**, *A9* (1), 1-27.

(92) Tidwell, P. W.; Mortimer, G. A. An Improved Method of Calculating Copolymerization Reactivity Ratios. *J. Polym. Sci., Part A: Polym. Chem.* **1965**, *3*, 369-387.

(93) Wiley, R. H.; Davis, B. Tracer Techniques for the Determination of Monomer Reactivity Ratios. IV. Monomer Reactivity Ratios for Styrene–Isoprene Copolymerization. *J. Polym. Sci., Part A: Polym. Chem.* **1963**, *1* (9), 2819-2830.

(94) Zverev, M. P.; Margaritova, M. F. Copolymerization of Isoprene and Styrene. *Urkrain. Khim. Zh.* **1958**, *24*, 626-628.

(95) Lewis, F. M.; Walling, C.; Cummings, W.; Briggs, E. R.; Wenisch, W. J. Copolymerization. VII. Copolymerizations of Some Further Monomer Pairs. *J. Am. Chem. Soc.* **1948**, *70* (4), 1527-1529.

(96) Gilbert, R. D.; Williams, H. L. Reactivity Ratios of Conjugated Dienes Copolymerized in Emulsion at 5 °C. *J. Am. Chem. Soc.* **1952**, *74* (16), 4114-4118.

(97) Crescentini, L.; Gechele, G. B.; Zanella, A. Butadiene/Styrene/2-Methyl-5-vinylpyridine Terpolymer. Composition-Conversion Data in Comparison with Calculated Values. *J. Appl. Polym. Sci.* **1965**, *9*, 1323-1340.

(98) Meehan, E. J. Composition of Butadiene-Styrene Copolymers Prepared by Emulsion Polymerization. *J. Polym. Sci., Part A: Polym. Chem.* **1946**, *1* (4), 318-328.

(99) Orr, R. J.; Williams, H. L. The Polymerization of Isoprene and 2,3-Dimethylbutadiene and Copolymerization with Styrene at – 18 °C. in Emulsion. *Can. J. Chem.* **1952**, *30*, 108-123.

(100) Orr, R. J. Thermochemical Aspects of Butadiene-Styrene Copolymerization. *Polymer* **1961**, *2*, 74-82.

(101) Mitchell, J. M.; Williams, H. L. Laboratory Study of Low Ratio Butadiene-Styrene Copolymers. *Can. J. Res.* **1949**, *27* (2), 35-46.

(102) Qiu, J.; Charleux, B.; Matyjaszewski, K. Controlled/Living Radical Polymerization in Aqueous Media: Homogeneous and Heterogeneous Systems. *Prog. Polym. Sci*. **2001**, *26* (10), 2083-2134.

(103) Kamachi, N.; Kajiwara, A. ESR Study on Radical Polymerizations of Diene Compounds. Determination of Propagation Rate Constants. *Macromolecules* **1996**, *29* (7), 2378-2382.

(104) Matheson, M. S.; Auer, E.E.; Bevilacqua, E. B.; Hart, E. J. Rate Constants in Free Radical Polymerization. III. Styrene. *J. Am. Chem. Soc.* **1951**, *73* (4), 1700-1706.

(105) Morton, M.; Salatiello, P. P.; Landfield, H. Absolute Propagation Rates in Emulsion Polymerization. III. Styrene and Isoprene. *J. Polym. Sci., Part A: Polym. Chem.* **1952**, *8* (3), 279-287.

(106) Greszta, D.; Matyjaszewski, K. Mechanism of Controlled/"Living" Radical Polymerization of Styrene in the Presence of Nitroxyl Radicals. Kinetics and Simulations. *Macromolecules* **1996**, *29* (24), 7661-7670.

(107) Kruse, T. M.; Souleimonova, R.; Cho, A.; Gray, M. K.; Torkelson, J. M.; Broadbelt, L. J. Limitations in the Synthesis of High Molecular Weight Polymers via Nitroxide-Mediated Controlled Radical Polymerization: Modeling Studies. *Macromolecules* **2003**, *36* (20), 7812-7823.

(108) Zetterlund, P. B.; Saka, Y.; McHale, R.; Nakamura, T.; Aldabbagh, F.; Okubo, M. Nitroxide-Mediated Radical Polymerization of Styrene: Experimental Evidence of Chain Transfer to Monomer. *Polymer* **2006**, *47* (23), 7900-7908.

(109) Nicolas, J.; Dire, C.; Mueller, L.; Belleney, J.; Charleux, B.; Marque, S. R. A.; Bertin, D.; Magnet, S.; Couvreur, L. Living Character of Polymer Chains Prepared via Nitroxide-Mediated Controlled Free-Radical Polymerization of Methyl Methacrylate in the Presence of a Small Amount of Styrene at Low Temperature. *Macromolecules* **2006**, *39* (24), 8274-8282.

(110) Petton, L.; Ciolino, A. E.; Dervaux, B.; Du Prez, F. E. From One-pot Stabilization to *In Situ* Functionalization in Nitroxide Mediated Polymerization: an Efficient Extension towards Atom Transfer Radical Polymerization. *Polym. Chem.* **2012**, *3*, 1867-1878.

(111) Nishizaki, H.; Yoshida, K. Effect of Molecular Weight on Various TGA Methods in Polystyrene Degradation. *J. Appl. Polym. Sci.* **1981**, 26, 3503-3504.

(112) Loadman, M. J. R. The Glass Transition Temperature of Natural Rubber. *J. Therm. Anal. Calorim.* **1985**, *30* (4), 929-941.

(113) Rieger, J. The Glass Transition Temperature of Polystyrene: Results of a Round Robin Test. *J. Therm. Anal. Calorim.* **1996**, *46* (3), 965-972.

(114) Georgopanos, P.; Rangou, S.; Haenelt, T. G.; Abetz, C.; Meyer, A.; Filiz, V.; Handge, U. A.; Abetz, V. Analysis of Glass Transition and Relaxation Processes of Low Molecular Weight Polystyrene-*b*-Polyisoprene Diblock Copolymers. *Colloid Polym. Sci.* **2014**, *292* (8), 1877-1891.

(115) Gedde, U. W. The Glassy Amorphous State. *Polymer Physics*; Kluwer Academic Publishers: Dordrecht, **1999**; 77-98.

(116) Tonelli, A. E. Possible Molecular Origin of Sequence Distribution-Glass Transition Effects in Copolymers. *Macromolecules* **1974**, *7* (5), 632-634.

(117) Michael, R. C. Glass Transition in Rubbery Materials. *Rubber Chemistry and Technology,* Vol. 85; ACS: Akron, **2012**; 3, 313-327.

(118) Halasa, A. F.; Jusinas, C.; Hsu, W. L.; Zanzig, D. J. Random Low Vinyl Styrene–Isoprene Copolymers. *Eur. Polym. J.* **2010**, *46*, 2013-2018. \